ANNUAL REVIEWS

Annual Review of Fluid Mechanics

Fluid-Elastic Interactions Near Contact at Low Reynolds Number

Bhargav Rallabandi

Department of Mechanical Engineering, University of California, Riverside, California, USA; email: bhargav@engr.ucr.edu

Annu. Rev. Fluid Mech. 2024. 56:491–519

First published as a Review in Advance on October 10, 2023

The *Annual Review of Fluid Mechanics* is online at fluid.annualreviews.org

https://doi.org/10.1146/annurev-fluid-120720-024426

Keywords

viscous flow, elasticity, fluid-structure interactions, lubrication

Abstract

Interactions between fluid flow and elastic structures are important in many naturally occurring and engineered systems. This review collects and organizes recent theoretical and experimental developments in understanding fluid-structure interactions at low Reynolds numbers. Particular attention is given to the motion of objects moving in close proximity to deformable soft materials and the ensuing interplay between fluid flow and elastic deformation. We discuss how this interplay can be understood in terms of forces and torques, and harnessed in applications such as microrheometry, tribology, and soft robotics. We then discuss the interaction of soft and wet objects close to contact, where intermolecular forces and surface roughness effects become important and are sources of complexity and opportunity.

1. INTRODUCTION

The interaction of fluid flow and deformable objects is a common feature of many physical systems. Flags flutter in the wind, fish swim, flagella beat to propel microorganisms, and blood cells bend and stretch as they squeeze through narrow capillaries. Flexible elements introduced into engineering fluidic channels can act as pumps and rectifiers. In this review, we summarize recent developments on the interactions of fluid flows and elastic structures, focusing on flows dominated by viscous forces. We discuss general principles by which suspended soft objects interact with each other and with nearby compliant structures. Such interactions arise in physiological contexts and in microscopic experiments with soft materials and have applications in microfluidics, soft robotics, rheometry, and tribology.

The interplay between fluid flow and deformable objects has a well-developed literature that spans a wide range of applications. Early work studied the role of deformations in industrial bearings under the large pressures of the lubricating fluid (Dowson & Higginson 1959, Archard et al. 1961, Crook 1961, Greenwood 2020). The role of deformability in the flow of red blood cells in capillaries was recognized in the mid-twentieth century (Lighthill 1968, Fitz-Gerald 1969). Subsequent work focused on the motion of deformable droplets in confined flows (Chan & Leal 1979, Yang & Leal 1990). In a now classic paper, Smart & Leighton (1991) showed that a droplet of radius R and surface tension σ in a wall-bounded shear flow with shear rate $\dot{\gamma}$ migrates away from the wall due to interfacial deformation. When the droplet is at a distance $d \gg R$ from the wall, the migration speed is

$$V_\perp \propto R\dot{\gamma}\left(\frac{R}{d}\right)^2 \mathcal{C}, \qquad 1.$$

where $\mathcal{C} = \mu R\dot{\gamma}/\sigma$ is the capillary number and controls the deformation of the drop from its spherical rest shape. This example of fluid-structure interaction exhibits many of the key features that we discuss in this article—stresses of the flow deform the object, and the deformed object then interacts hydrodynamically with a nearby boundary, which in turn modifies the motion of the particle.

There has been growing recent interest in the motion of suspended objects in close proximity to soft materials (often elastomers or gels) with elastic, viscoelastic, or poroelastic properties. The large hydrodynamic stresses typical of near-contact configurations can thus produce a strong coupling between fluid flow and elastic deformation. Moreover, the close proximity between compliant surfaces, particularly at nanometric surface separation distances, can cause intermolecular forces and surface roughness effects to become important. It is in this context that the present review discusses fluid-elastic interactions. We focus primarily on situations where the interacting soft objects are in close proximity to each other and fluid-elastic interactions are relatively strong. In this regime, the ideas of lubrication theory are effective and afford significant simplifications of both the fluid dynamics and the solid mechanics.

We first discuss the motion of particles near soft boundaries, detailing the generation of forces due to nonlinear effects of soft materials (Section 2) as well as a linearized description of time-dependent motion that is useful for microrheometry (Section 3). We then discuss situations in which soft objects undergo relative sliding while simultaneously being pressed together (Section 4). We are then naturally led to a discussion of the hydrodynamics of approach and contact of soft objects, including the role of intermolecular forces, which we discuss in Section 5. Connections to other soft hydrodynamic systems are made in Section 6 before we conclude in Section 7.

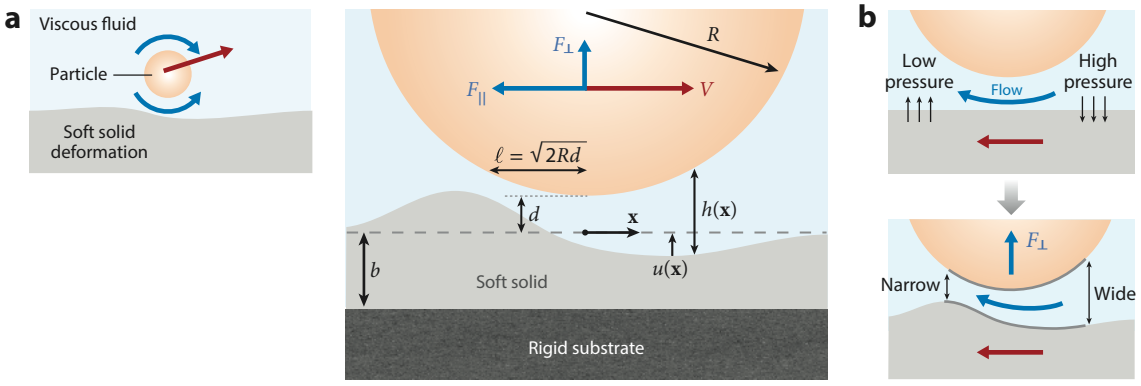

Figure 1

Mechanism of normal force generation due to sliding of a symmetric object along a soft solid. (*a*) Fluid-elastic interactions between objects in close proximity are often well described under the framework of lubrication theory. (*b*) The flow generated by the object deforms the soft material in such a way that, in a reference frame attached to the object, fluid flows from wider regions of the film into narrower regions. This generates a net positive pressure in the fluid film, producing an normal force on the object.

2. FORCES ON PARTICLES TRANSLATING NEAR COMPLIANT SURFACES

We begin by discussing the motion of suspended particles moving near compliant surfaces. When a particle translates close to a rigid boundary, it experiences hydrodynamic forces and torques that depend on its distance to the boundary (Kim & Karrila 2013). If this boundary is instead compliant, the motion of the particle drives a fluid flow whose stresses deform the boundary, which in turn produces a secondary flow. The effects of this secondary (deformation-induced) flow can be felt by the particle in multiple ways. When the particle motion is prescribed, the particle experiences additional elastohydrodynamic (EH) components of force or torque that depend on the stiffness of the materials (Coyle 1988, Sekimoto & Leibler 1993, Skotheim & Mahadevan 2004, Yin & Kumar 2005). Alternatively, if the particle is freely suspended, then these interactions manifest as elasticity-dependent modifications of the particle's kinematics (**Figure 1*a***). Notable among these effects is the lowering of the effective friction between sliding soft objects (Saintyves et al. 2016), the drift of translating particles away from soft boundaries (Davies et al. 2018, Rallabandi et al. 2018), or coupling between translation and rotation (Salez & Mahadevan 2015, Rallabandi et al. 2017, Saintyves et al. 2020). We point the reader to the recent review by Bureau et al. (2023), which discusses several mechanisms by which particles may cross streamlines in viscous flows, including those resulting from elastic deformations.

At low Reynolds numbers, stresses generated by the motion of the particle fall off with the inverse square of the distance from the particle (or faster). It is therefore typical to consider situations in which the separation distance d is not too large relative to the radius of the particle R in order for the effects of boundary deformations to be felt appreciably. For very small separation distances $d \ll R$, lubrication theory provides a simplified, yet often accurate, description of the fluid flow. The fluid flow is driven by pressure gradients ∇p along the film, and by the relative motion between the surfaces (**Figure 1*a***). For a Newtonian fluid of viscosity μ, and for objects sliding with relative velocity $\mathbf{V}$, the flow is governed by

$$\frac{\partial h}{\partial t} = \frac{1}{12\mu}\nabla \cdot \left(h^3 \nabla p + 6h\mathbf{V}\right), \qquad 2.$$

where $h(\mathbf{x}, t)$ is the width of the fluid gap (which we also refer to as the fluid film thickness) and depends on the location in the plane $\mathbf{x}$ and can evolve in time t. The film thickness can be decomposed into a contribution $h^{\text{rigid}}(\mathbf{x}, t)$ from the surfaces in their undeformed state and a contribution $u(\mathbf{x}, t)$ due to elastic deformation. Around the point of minimum separation and in the undeformed configuration, it is typical to describe spherical and cylindrical objects by a parabolic approximation $h^{\text{rigid}} \simeq d(t) + |\mathbf{x}|^2/(2R)$, where $d(t)$ is the minimum separation distance between the undeformed surfaces of the particle and the wall. Thus, the film thickness typically has the shape

$$h(\mathbf{x}, t) \simeq d(t) + \frac{|\mathbf{x}|^2}{2R} + u(\mathbf{x}, t) \qquad 3.$$

The surface deformation field $u(\mathbf{x}, t)$ (defined such that positive u widens the gap) is coupled to stresses of the fluid flow via the equilibrium of elastic stresses in the soft material. Shear stresses are smaller than normal stresses in lubricated flows and are typically neglected, whereas normal stresses are dominated by pressure. For linearly elastic materials, the pressure of the flow and the surface deformation are typically related by

$$u(\mathbf{x}, t) = \int p(\mathbf{y}, t)\, \mathcal{G}(\mathbf{x} - \mathbf{y})\, \mathrm{d}^2\mathbf{y}. \qquad 4.$$

Here, $\mathcal{G}(\mathbf{x} - \mathbf{y})$ is a point response function that relates the deformation at $\mathbf{x}$ to a normal point force applied at $\mathbf{y}$ (also in the plane of the undeformed surface) and depends on the properties of the soft solid. Together, Equations 2–4 constitute a nonlinear description of EH interactions for closely separated surfaces and, as we show, provide quantitative insight into various EH phenomena in practically relevant scenarios. A more general EH framework replaces Equation 2 by the Stokes equations and Equation 4 by an elastic description involving both tangential and normal stresses and displacements (e.g., Hu et al. 2023).

2.1. Steady Sliding: The Generation of Normal Forces

A widely studied configuration involves a rigid symmetric particle (e.g., a cylinder or a sphere) translating parallel to a soft substrate that is planar in its undeformed equilibrium state. An important feature of this configuration is the generation of EH force components that are normal to the direction of motion (these normal forces are often referred to as lift forces; we use the two terms interchangeably here). By contrast, no normal force is experienced by the particle if the surface is rigid, as is expected from the time-reversal symmetry of Stokes flows (**Figure 1*b***).

2.1.1. Scaling and symmetry breaking. The locally parabolic geometry defines a horizontal length scale $\ell = \sqrt{2Rd}$ (**Figure 1*a***). In a reference frame attached to the particle, the wall appears to translate with velocity $-\mathbf{V}$, and the flow appears steady. The lubrication pressure scale is $p \sim \mu V \ell/d^2$ and produces elastic deformations. We imagine that strains in the material are distributed over a region of a characteristic horizontal length scale ℓ_s, which may depend on the geometric scale ℓ, as well as the properties of the soft material. This leads to a characteristic elastic stress Ku/ℓ_s, where K is an effective elastic modulus with units of force per area [these details are contained within the response function $\mathcal{G}(\mathbf{r})$ in Equation 4]. Balancing the elastic stress with the pressure of the fluid leads to a deformation scale $u \sim p\ell_s/K$. The ratio of the deformation scale and the separation distance d defines a dimensionless parameter

$$\eta = \frac{\mu V \ell \ell_s}{K d^3} = \frac{\mu V (2R)^{1/2} \ell_s}{K d^{5/2}}. \qquad 5.$$

This quantity can be interpreted either as a dimensionless velocity or as a dimensionless elastic compliance. In the latter interpretation, η is analogous to the capillary number in that it provides a measure of the effect of hydrodynamic forces on deformation; $\eta = 0$ is the rigid limit.

In the rigid (and symmetric) configuration, the time-reversal symmetry of Stokes flows precludes the generation of any normal forces from translation parallel to a wall. However, in the deformed configuration, fluid flows on average from a wider section of the gap (ahead of the particle; the inlet) into a narrower section (behind the particle; the outlet) (see **Figure 1*b***). Elastic deformation due to flow thus breaks symmetry and generates a nonzero mean secondary pressure in the gap that then leads to a normal force. Adopting arguments relevant to slider bearings (Reynolds 1886), we expect this normal force to push the surfaces apart. For small sliding speeds, the secondary pressure has a scale $\eta\mu V\ell/d^2$, which depends on both the elastic and fluid properties. The resulting EH lift force (on a sphere) thus scales as

$$F_\perp^{\mathrm{EH}} = \int p\,\mathrm{d}A \sim \int \eta \frac{\mu V \ell}{d^2}\,\mathrm{d}A \sim \frac{\mu^2 V^2 R^2 \ell_s}{K d^3}. \qquad 6.$$

For a cylinder, the force per length scales with the result of Equation 6 divided by ℓ. The same symmetry arguments are relevant to the motion of drops near walls and particles near free surfaces (Berdan & Leal 1982, Yang & Leal 1990).

Translation of a particle parallel to a compliant wall therefore generates a force component normal to the wall. This force is quadratic in the sliding speed for small speeds. Detailed calculations show that the force is repulsive, as argued above. The motion of soft spherical particles is similar in principle but with some caveats that we discuss separately in Section 2.4. Below, we highlight theoretical quantifications of the nonlinear EH lift force and its manifestations in experiments.

2.1.2. Thin, compressible, elastic layers and the Winkler approximation. The simplest elastic model is that of a Winkler mattress (or foundation), which treats the soft material as a bed of isolated springs. Such a response is physically realized by a thin, compressible, soft layer (of thickness $b \ll \ell$, shear modulus G, and Poisson's ratio ν) bonded to a rigid substrate. In this case, the surface deformation is related to pressure by

$$u = \frac{b(1-2\nu)}{2(1-\nu)G} p. \qquad 7.$$

Here, the layer thickness b can be identified with the length scale ℓ_s over which elastic stresses are distributed, and $K = 2G(1-\nu)/(1-2\nu)$ is the effective stiffness introduced in Section 2.1.1. Owing to its simplicity, the Winkler model is widely applied and often provides useful qualitative insights into soft systems, including those with quite complex elastic responses (Dillard et al. 2018). For a cylinder sliding along a Winkler mattress at steady state, Equation 2 becomes

$$\frac{\mathrm{d}}{\mathrm{d}x}\left(\left(d + \frac{x^2}{2R} + \frac{b}{K}p\right)^3 \frac{\mathrm{d}p}{\mathrm{d}x} + 6\mu V\left(d + \frac{x^2}{2R} + \frac{b}{K}p\right)\right) = 0, \qquad 8.$$

which is a second-order nonlinear differential equation for the pressure $p(x)$. Rescaling identifies the compliance $\eta = \mu V b\ell/(Kd^3)$, which is the sole parameter of the problem.

For small η, the pressure is largely antisymmetric and corresponds to motion between nearly rigid surfaces. As η increases (softer materials or faster speeds), the pressure and the deformation become asymmetric about the origin. For small deformations, Equation 8 yields readily to a perturbation expansion of the form $p(x) \sim p_0(x) + \eta p_1(x) + \ldots$, which can be solved order by order. The normal force (per length) on the cylinder is $F_\perp^{\mathrm{EH}} = \int_{-\infty}^{\infty} p(x)\mathrm{d}x$, to which the leading term p_0 (flow between undeformed surfaces) makes no contribution due to symmetry. The next term, ηp_1, breaks this symmetry and gives rise to a normal force (per length) (Sekimoto & Leibler 1993, Skotheim & Mahadevan 2004)

$$F_\perp^{\mathrm{EH}} = \int_{-\infty}^{\infty} p\,\mathrm{d}x \sim \frac{3\pi}{8}\eta\frac{\mu V\ell}{d^2}\ell = \frac{(1-2\nu)}{1-\nu}\frac{3\sqrt{2}\pi}{8}\frac{\mu^2 V^2 b R^{3/2}}{G d^{7/2}}. \qquad 9.$$

A numerical solution of Equation 8 finds that the approximation 9 is accurate to within about 10% when $\eta \lesssim 0.2$ (Skotheim & Mahadevan 2004). A similar approach also yields the normal force on a spherical particle sliding near a Winkler foundation (Urzay et al. 2007), though the algebra is considerably more involved. In two-dimensional configurations, the normal force typically achieves a maximum value for intermediate values of η (Beaucourt et al. 2004, Skotheim & Mahadevan 2005), but this feature seems to disappear for spherical geometries (Urzay et al. 2007) and simply saturates for $\eta \gtrsim 1$.

2.1.3. Elastic layers: beyond the Winkler approximation. Most soft materials found in the laboratory and in nature (e.g., elastomers and gels) are nearly incompressible. For a strictly incompressible material (Poisson's ratio $\nu = 1/2$), the Winkler model predicts an infinite resistance to deformation and must be replaced by more sophisticated descriptions. For thin incompressible layers, surface displacements are accommodated as shear strains, leading to $u \propto -b^3 \nabla^2 p/G$ (this can be recast in terms of Equation 4 through a Green's function formulation). The symmetry arguments continue to hold, whereas the scaling behaviors with respect to geometric parameters are modified. Accounting for both compression and shear of thin layers, Chandler & Vella (2020) found a transition between compressible and incompressible scaling behaviors for the EH lift force when $b/\ell \sim \sqrt{1-2\nu}$. For thicker elastic substrates, it is necessary to use the full integral relation given by Equation 4. Recently, Hu et al. (2023) showed that for a very thin incompressible elastic layer of thickness comparable to that of the fluid film ($b \lesssim d$), the shear stress of the flow (despite being smaller than the pressure) produces sizable elastic deformations. Accounting for this effect further modifies the scaling of the lift force in this limit. Another useful limit is that of a substrate that is much thicker than the geometry of contact ($b \gg \ell$), where elastic stresses are distributed over a region of size $\ell_s \sim \ell$, and the response kernel is $\mathcal{G}(\mathbf{r}) \propto G^{-1}|\mathbf{r}|^{-1}$ (in three dimensions) and $\mathcal{G}(\mathbf{r}) \propto G^{-1} \log|\mathbf{r}|$ in (two dimensions) (Johnson 1987). Coupling the Reynolds Equation 2 to the pressure-displacement relation (Equation 4) results in a nonlinear integrodifferential equation that must be solved numerically in general. Skotheim & Mahadevan (2005) develop and document an extensive library of both analytic and numerical results for lift forces in a wide range of two-dimensional configurations.

There is a smaller literature on spherical geometries, but we note the work of Urzay et al. (2007) in the Winkler limit and the recent work by Zhang et al. (2020) that analyzed the lift on a sphere translating near a thick, soft substrate using a semianalytical perturbation approach. An alternative strategy, valid for small displacements, is to use the Lorentz reciprocal theorem to obtain the lift force while circumventing the details of the secondary pressure field (for an overview of the theorem and its applications, see Masoud & Stone 2019). The idea was first introduced by Stone et al. (2004) in the context of the Winkler model and has since been generalized to more complex elastic responses. The method utilizes well-known solutions of the Stokes equations in rigid geometries along with approximations of the deformation to compute the lift force. Working in Fourier space (and building on the theory of Rallabandi et al. 2018), Kargar-Estahbanati & Rallabandi (2021) showed that the EH normal force on a sphere, accurate to leading order in deformation, has the general form

$$F_{\perp}^{\mathrm{EH}} = \frac{9\mu^2 V^2 R^{5/2}}{25\sqrt{2}\, d^{5/2}} \int q^4 \left\{K_0(q)\right\}^2 \tilde{\mathcal{G}}^*(\mathbf{q})\, \mathrm{d}^2\mathbf{q}, \qquad 10.$$

where K_0 is a modified Bessel function. The quantity $\tilde{\mathcal{G}}(\mathbf{q}) = \int \mathcal{G}(\mathbf{r}) \mathrm{e}^{-\mathrm{i}\mathbf{q}\cdot\mathbf{r}} \mathrm{d}^2\mathbf{r}$ is the Fourier transform of the Green's function (the asterisk in Equation 10 represents a complex conjugate) and is known analytically in many systems (Li & Chou 1997, O'Sullivan & King 1988, Wang & Zhu 2019).

To close this section, we note that if the object rotates, it is appropriate to replace **V** by a combination of translation and rotation velocities (the entrainment velocity) in the Reynolds lubrication equation. However, we note that forces and torques depend separately on rotational and translational velocities (see Urzay et al. 2007, Rallabandi et al. 2017, Bertin et al. 2022).

2.2. Experimental Quantification of Nonlinear Elastohydrodynamic Normal Forces

A small but growing body of experimental literature has confirmed the generation of normal forces on suspended particles near soft materials. Saintyves et al. (2016) made perhaps the first quantitative experimental measurements of EH lift effects by studying the sliding of rigid submerged cylinders over inclines coated with elastomers (**Figure 2*a***). The EH lift force slightly separates the cylinder from the soft surface, which lowers the drag on the cylinder (recall that the drag force per length on a cylinder scales as $\mu V\ell/d$). At steady state, the separation distance and the sliding speed are simultaneously determined by a balance of the weight of the cylinder, hydrodynamic drag, and EH lift. The sliding speed was found to be greater for softer coatings according to $V \propto G^{-1/5}$, in agreement with small-deformation theory under the Winkler approximation (**Figure 2*b***).

In another macroscopic experiment, Rallabandi et al. (2018) showed that particles settling near taut, vertically suspended elastic sheets drift away from the sheet (**Figure 2*c***). Neglecting geometric nonlinearities associated with sheet bending, they modeled the deformations of the sheet via

$$(B\nabla^4 - T\nabla^2)u = p, \qquad 11.$$

where $B = Gb^3(1 + \nu)/(6(1 - \nu^2))$ is the bending rigidity and T is the applied tension. The motion of the particle along the sheet produces an EH lift that is balanced by a drag normal to the surface, establishing a normal drift velocity (**Figure 2*d***)

$$V_\perp = \frac{3\mu R^2 V^2}{25B}\mathcal{F}\left(\frac{2TRd}{B}\right), \quad \text{where} \quad \mathcal{F}(\mathcal{T}) = \int_0^\infty \frac{2q^4K_0^2(q)}{q^4 + \mathcal{T}q^2}q\mathrm{d}q. \qquad 12.$$

The function $\mathcal{F}$ depends on the dimensionless ratio $\mathcal{T} = 2TRd/B$, which quantifies the relative importance of tension to bending rigidity in resisting deformation. Motivated by particle motion near biological membranes, Daddi-Moussa-Ider et al. (2018) analyzed nonlinear elastohydrodynamic lubrication (EHL) forces experienced by a particle translating far away from a planar membrane ($d \gg R$) with resistance to bending and in-plane shear (Helfrich 1973, Skalak et al. 1973, Tözeren & Skalak 1978). While bending resulted in a repulsive interaction, resistance to in-plane straining was predicted to produce an attractive interaction.

Other recent experiments have either directly or indirectly measured EH lift effects at the microscale. Davies et al. (2018) flowed heavy spherical particles in a microchannel whose bottom wall was functionalized with polymer brushes. The particles were observed to flow at different heights above the brush layer depending on the shear rate of the flow (which controlled both translation and rotation of the particles) and the stiffness of the brushes (**Figure 3*a***). These observations were shown to be in quantitative agreement with a balance between the weight of the particles and EHL forces, with a smaller contribution from inertial effects. Vialar et al. (2019) measured normal forces between sliding mica-bead-coated surfaces using a surface force apparatus (SFA), finding qualitative agreements with the EH lift theory (**Figure 3*b***). The following year, Zhang et al. (2020) performed direct measurements of the EH lift force using an atomic force microscope with a spherical probe near a transversely oscillating stage coated with polydimethylsiloxane (PDMS). Due to the quadratic nonlinearity, transverse oscillations generate a normal EH force component with nonzero mean that scales as $d^{-5/2}$, in agreement with (quasi-static) theory for small deformations (**Figure 3*c***). Evaluation of Equation 10 (Kargar-Estahbanati & Rallabandi

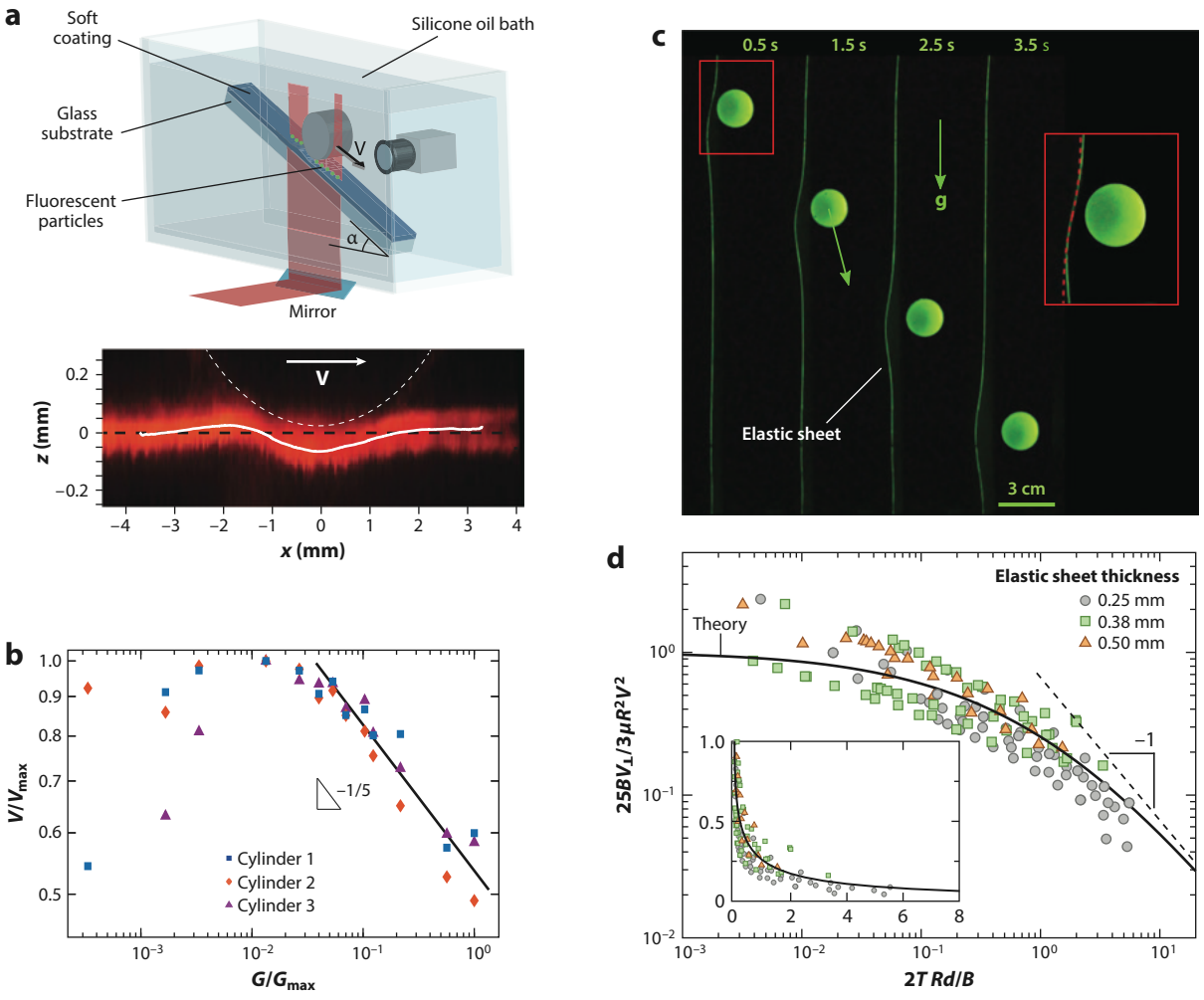

Figure 2

(*a*) A cylinder sliding along a soft incline experiences an elastohydrodynamic (EH) lift force that counteracts its weight. As a result, the cylinder glides a small distance above the surface. (*b*) Softer materials lead to faster sliding. (*c*) A particle sedimenting near a vertically suspended elastic membrane drifts away from it. (*d*) The drift speed of the particle away from the membrane, $V_\perp$, depends on the tension (T) and bending rigidity (B) of the sheet for different experimental conditions (*symbols*) and is well captured by EH lubrication theory (*curve*). Panels adapted with permission from (*a*,*b*) Saintyves et al. (2016) and (*c*,*d*) Rallabandi et al. (2018).

2021) quantifies deviations from this scaling behavior depending on the thickness of the soft layer (**Figure 3*d***).

2.3. Effect of Substrate Viscoelasticity

Many soft materials exhibit viscoelastic properties, which can affect EH forces. The ratio of the material relaxation timescale τ to the advection timescale ℓ/V gives rise to a new dimensionless parameter. When $\tau \gtrsim \ell/V$, the material cannot respond instantaneously to the moving object. This produces deformations that are both smaller and more symmetric (**Figure 3*e***), which leads to a smaller normal force than the purely elastic case (Pandey et al. 2016, Hu et al. 2023). When

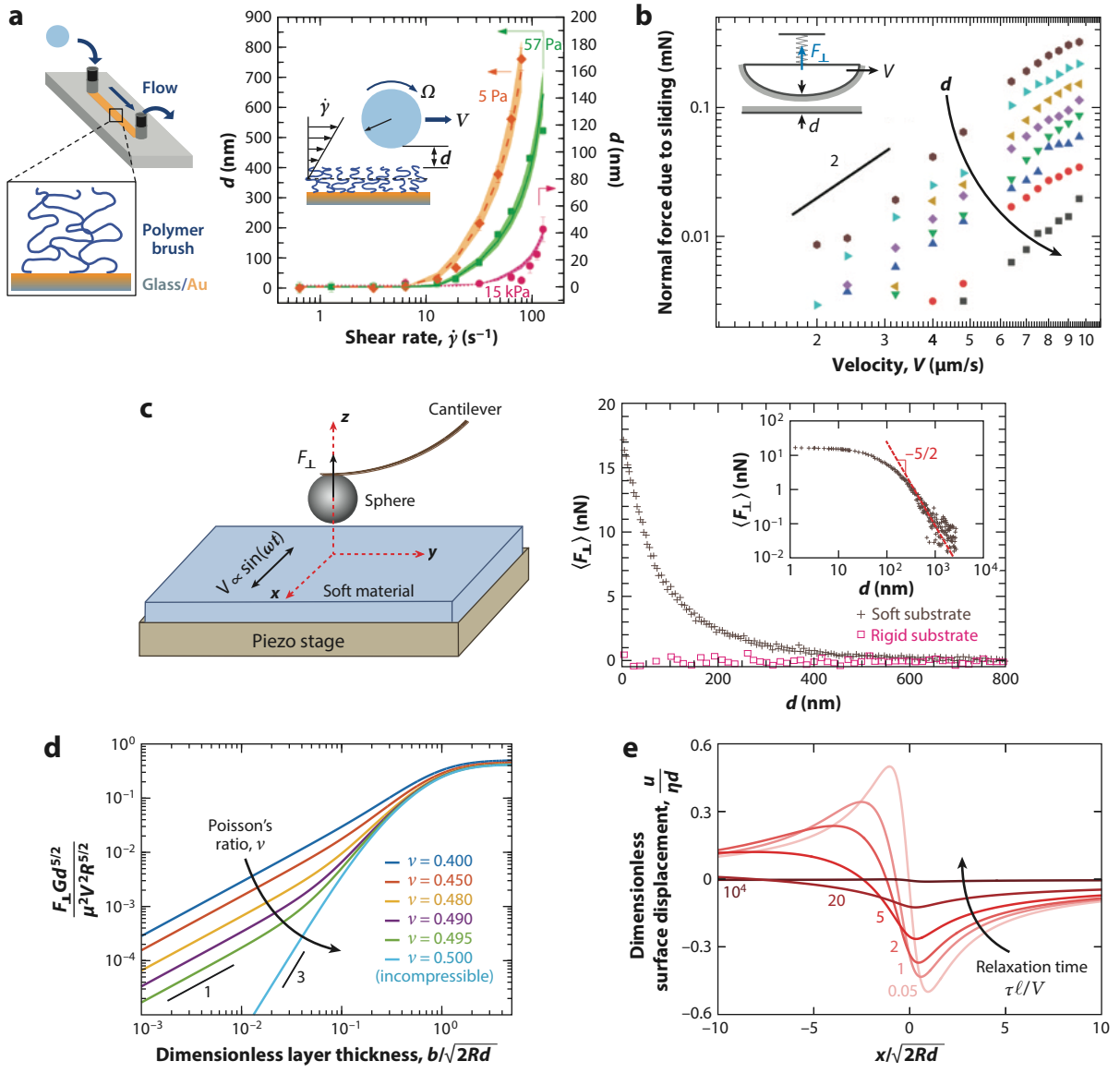

Figure 3

(*a*) Particles flowing in polymer-coated microchannels assume a steady-state separation distance *d*, established by a balance of elastohydrodynamic (EH) lift, an inertial lift, and the weight of the particles. Data are shown for polymer coatings of different stiffness $2G(1-\nu)/(1-2\nu)$. (*b*) Lateral sliding between microgel-coated surfaces leads to a normal force that is quadratic in the sliding speed and decreases with increasing separation distance *d* (e.g., *brown hexagons*: 130 nm; *black squares*: 300 nm). (*c*) Lateral oscillations of a polydimethylsiloxane substrate produce a time averaged normal force on a spherical atomic force microscopy probe. The force decays as $d^{-5/2}$, in agreement with theory. (*d*) Dependence of the EH lift force on layer thickness and Poisson's ratio, showing two distinct scaling regimes for thin layers. (*e*) For viscoelastic materials, larger relaxation times lead to smaller deformations and therefore smaller lift forces. Panels adapted with permission from (*a*) Davies et al. (2018), (*b*) Vialar et al. (2019), (*c*) Zhang et al. (2020), (*d*) Kargar-Estahbanati & Rallabandi (2021), and (*e*) Pandey et al. (2016).

the translation is oscillatory (as in Zhang et al. 2020) with frequency ω, the nonlinear normal force $F_{\perp}^{EH}(t)$ is a superposition of steady and overtone (2ω) components for small η. For a viscoelastic substrate, the amplitude and phase information of this force signal are predicted to be tied to the storage and loss moduli of the material (Kargar-Estahbanati & Rallabandi 2021).

2.4. Deformable Particles and the Role of Particle Shape

The ideas discussed above also apply in principle to soft objects translating near rigid walls. Indeed, for symmetric vesicles, Beaucourt et al. (2004) found a repulsive force consistent with EH theory. However, for nonspherical particles, elastic deformations may play only a subdominant role in geometric symmetry breaking. One example is that of a nonspherical vesicle exposed to shear flow near a wall, which under certain conditions assumes an ellipsoidal shape at a constant angle with respect to the wall (the shear flow tries to reorient the vesicle along the directions of principal strain) and drifts away from it (Abkarian et al. 2002). Approximating the vesicle by a point stresslet (valid when $d \gg R$) with a wall-normal component Σ_{zz} leads to the prediction

$$V_{\perp} = \frac{9\Sigma_{zz}}{64\pi\mu d^2} \propto \frac{\dot{\gamma} R^3}{d^3} + \text{ deformability effects}, \qquad 13.$$

which agrees with experiments and simulations over a wide range of conditions (Abkarian et al. 2002, Zhao et al. 2011). To first approximation, Σ_{zz} is linear in the shear rate and depends on the asphericity of the vesicle, while elastic deformations make a sub-dominant contribution (e.g., Bureau et al. 2023). Note that the stresslet argument also applies to a droplet near a wall (see Equation 1), except that in this case the dominant contribution to the stresslet occurs precisely due to deformation of the droplet by the flow against surface tension (Smart & Leighton 1991).

3. LINEARIZED PARTICLE DYNAMICS NEAR SOFT MATERIALS

In the preceding section we discussed the generation of normal forces due to quasi-static wall-parallel translation. Such forces are (for small velocities) quadratic in the velocity and linear in the elastic compliance $1/G$ and are associated with the breaking of geometric symmetry. However, when the motion is time dependent, the kinematics of boundary deformation generate additional force components that are linear in velocity. This leads to mobility relations of the kind familiar in viscous hydrodynamics (Hinch 1972) but now involving the properties of the soft material. The elastic contribution to the force response depends on the timescales over which the system is probed relative to a relaxation time μ/G (modulo geometric factors). We discuss some examples of such systems below.

3.1. Oscillations Normal to a Soft Material: Contactless Rheometry

Accurately measuring the mechanical properties of a soft material can be challenging at small scales. Traditional mechanical tests (e.g., indentation) are prone to contamination by adhesive, capillary, and intermolecular forces, particularly for soft materials. To overcome these challenges, Leroy & Charlaix (2011) and Leroy et al. (2012) devised theory and experiments to use fluid-elastic interactions to probe the mechanical response of a soft material without direct solid-to-solid contact. Their setup consists of an SFA involving a spherical probe that is suspended at a known height d_0 above a layer of soft material, separated by viscous fluid. Vertical oscillations of amplitude $A \ll d_0$ and frequency ω are then applied to the probe, so that the separation distance between the (undeformed) surfaces is $d(t) = d_0 + Ae^{i\omega t}$ (**Figure 4*a***). The ensuing flow deforms the soft material, and thus, the force exerted by the fluid on the particle (which can be measured) carries an imprint of the mechanical properties of the soft solid.

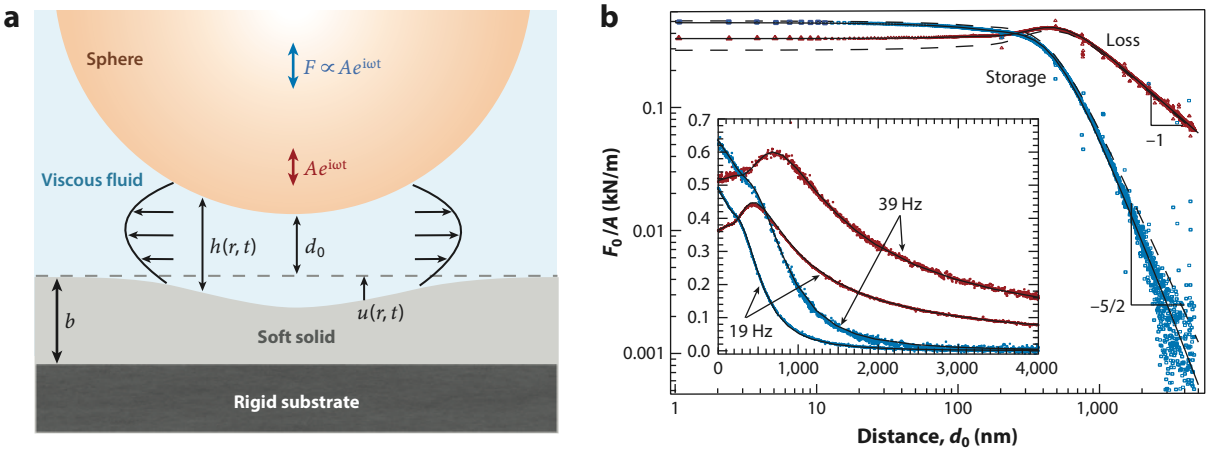

Figure 4

(*a*) Small vertical oscillations of a sphere about a mean separation distance d_0 deform a nearby elastic material. (*b*) The normal force on the sphere has components in phase (*blue*) and out of phase (*red*) with the displacement, corresponding to elastic (storage) and viscous (loss) contributions, respectively. Theory is shown as solid black curves; dashed curves correspond to the limit of a thick elastic substrate. The inset shows the same data on linear axes. Panel *b* adapted with permission from Leroy et al. (2012).

The theory of Leroy & Charlaix (2011) linearizes the lubrication equation in the oscillation amplitude, allowing for changes of film thickness due to elastic deformation. The linearized Reynolds equation around a sphere, assuming axisymmetric flow, is

$$\frac{\partial}{\partial t}\left(d_0 + A\mathrm{e}^{\mathrm{i}\omega t} + u\right) = \frac{1}{12\mu}\frac{1}{r}\frac{\partial}{\partial r}\left(\left(d_0 + \frac{r^2}{2R}\right)^3 \frac{\partial p}{\partial r}\right), \qquad 14.$$

subject to the integral relation Equation 4 that links u to p. A Fourier transform in time and Hankel transform in space produces a Fredholm integral equation of the second kind for the (transformed) pressure that, when solved numerically, yields the normal force. The pressure scale due to a normal velocity $A\omega$ is $\mu A\omega\ell^2/d_0^3$, which leads to a deformation scale (for a thick elastic substrate) of $\mu A\omega\ell^3/(Gd_0^3)$. The deformation becomes comparable to the oscillation amplitude A (while remaining much smaller than d_0) for a characteristic separation distance (utilizing $\ell = \sqrt{2d_0R}$) of $d_c \sim R(\mu\omega/G)^{2/3}$. The ratio $d_0/d_c = (\mu\omega/G)^{-2/3}(d_0/R)$ is the sole dimensionless parameter of the system and characterizes the amplitude of deformation to that of the sphere oscillations (note that the deformations are assumed small relative to the gap d_0 throughout). The quantity $(d_0/d_c)^{-3/2} = (\mu\omega/G)(d_0/R)^{3/2}$ is the ratio of a relaxation timescale to the driving timescale and can be loosely interpreted as the Deborah number of the coupled fluid-elastic system (Ewoldt & Saengow 2022).

In this linear theory, the normal force on the particle also oscillates at frequency ω and has the general form (Leroy & Charlaix 2011)

$$F_\perp(t) = F_0\mathrm{e}^{\mathrm{i}\omega t}, \quad \text{where} \quad F_0 = \frac{6\pi\mu R^2 A\omega}{d_c}\mathcal{R}\left(\frac{d_0}{d_c}\right) \qquad 15.$$

The dimensionless resistance $\mathcal{R}(d_0/d_c)$ is a complex function whose real and imaginary parts represent elastic (storage) and viscous (loss) components. For example, when $d_0/d_c \gg 1$ (large separations or small frequencies) with a substrate much thicker than $\sqrt{Rd_0}$, the resistance takes the form $\mathcal{R}(d_0/d_c) \sim \mathrm{i}d_c/d_0 + 0.173\,(d_c/d_0)^{5/2}$, which corresponds to the viscous resistance on a sphere moving normal to a wall (Brenner 1961), plus an elastic correction scaling with $d_0^{-5/2}$ (**Figure 4*b***). For small d_0, the force is controlled entirely by d_c and becomes independent of the

gap width d_0. The crossover between storage and loss components of the resistance occurs when $d_0/d_c = O(1)$.

Experimental measurements of the force (Leroy et al. 2012) with an SFA find remarkable agreement with the theory across the entire range of experimentally accessed d_0/d_c (**Figure 4*b***), for both compressible and incompressible elastic responses. Bertin et al. (2022) analyzed the arbitrary time-dependent motion (translation and rotation) of a sphere near an elastic substrate, focusing on the quasi-steady limit (large d_0/d_c in the discussion above). Notably, they showed that the EHL forces and torques also depend on the acceleration of the particle, which, although reminiscent of inertial effects, arises due to the coupling between viscous flow and elastic deformation.

Similar ideas have since been used to probe the viscoelastic properties of polymer films (Guan et al. 2017a), cells (Guan et al. 2017b), fluid interfaces (Maali et al. 2017, Bertin et al. 2021), and gels (Zhang et al. 2022), in these instances using atomic force microscopy (AFM). Recent theoretical work (Kopecz-Muller et al. 2023) has analyzed the effects of poroelasticity in oscillating probe systems. For both viscoelastic and poroelastic materials, it is now necessary to sweep across an additional parameter $\omega\tau$ that depends on the material relaxation time τ. Experiments are somewhat complicated by the involvement of the driving frequency in both dimensionless parameters of the system (d_0/d_c and $\omega\tau$) but remain tractable.

SFA and AFM systems driving normal oscillations are promising as noncontact microrheological probes of soft materials, as they do not rely on weak nonlinearities or a breaking of symmetry (contrast this with Section 2.1). However, the force signal is at the same frequency as the driving and must be picked apart from purely hydrodynamic contributions to isolate elastic effects. By contrast, exploiting nonlinear interactions (e.g., Zhang et al. 2020) yields time-averaged and second harmonic signals that isolate EH effects but may be weaker and therefore more prone to contamination by noise. It is conceivable that a combined analysis of linear and nonlinear effects may provide an effective strategy for the microrheometry of complex soft solids.

3.2. Point-Like Particles near Interfaces and Membranes

There is an extensive body of work seeking to understand the properties of fluid interfaces and biological membranes by observing the motion of nearby suspended particles, or by direct observations of the fluctuations of interfaces themselves. It is well known that thermal fluctuations of lipid bilayer membranes are intimately coupled with the surrounding fluid (Brochard & Lennon 1975, Ramaswamy et al. 1994, Zilman & Granek 1996). Later work identified that nearby suspended particles are affected by these membrane fluctuations, leading to anomalous diffusion of the particles (Fradin et al. 2003, Kimura et al. 2005).

Recent years have seen theoretical efforts quantifying the mobility of particles near membranes (Bickel 2007, Daddi-Moussa-Ider et al. 2017) including hydrodynamic interactions between particles (Daddi-Moussa-Ider & Gekle 2016). The typical formulation treats the particle as small relative to its distance from the membrane ($R \ll d$), approximating it as a point-like object. The fluid flow [velocity $\mathbf{v}(\mathbf{x})$] is governed by the Stokes equations driven by a point force $\mathbf{F}$ at the location $\mathbf{x}_p$ of the particle,

$$\mu\nabla^2\mathbf{v} - \nabla p + \mathbf{F}\delta(\mathbf{x} - \mathbf{x}_p) = \mathbf{0}, \quad \text{with} \quad \nabla\cdot\mathbf{v} = 0. \tag{16.}$$

Kinematic and stress conditions couple the fluid flow to the elasticity of the membrane, which may resist both in-plane (shearing) and out-of-plane (bending) deformations. This time, the coupling of boundary deformations to fluid flow introduces a timescale $\mu d^3/B$. For small deformations, the particle velocity is related to applied forces $\mathbf{F} \propto e^{i\omega t}$ (it proves convenient to work in Fourier

space) through the linear relation

$$\mathbf{V} = \boldsymbol{\mathcal{M}}\left(\frac{d}{R}, \frac{\mu d^3 \omega}{B}, \ldots\right) \cdot \mathbf{F}. \qquad 17.$$

The mobility tensor $\boldsymbol{\mathcal{M}}$ is a complex quantity whose real (imaginary) parts describe viscous (elastic) contributions. The mobility depends on the dimensionless distance to the membrane d/R and a dimensionless frequency $\mu d^3\omega/B$, among other quantities involving the membrane tension or the in-plane shear modulus. Such descriptions have been used to study the diffusion of particles near membranes (Bickel 2006, Daddi-Moussa-Ider et al. 2016) and have predicted anomalous diffusion behavior, including long-lived subdiffusive transients.

Similar ideas have been developed for noncontact interfacial rheometry of complex fluid interfaces and monolayers (for a review of interfacial rheology, see Manikantan & Squires 2020). The idea is to suspend a submerged micron-sized bead in an optical trap close to an interface and use observations of its thermal fluctuations to infer properties of the interface. Shlomovitz et al. (2013) and Boatwright et al. (2014) developed theory and experiments, respectively, for how such particle fluctuations are coupled with the interface, focusing on the effects of interfacial viscosity in the plane of the interface but neglecting out-of-plane deflections.

4. LUBRICATED SLIDING BETWEEN CONFORMING SOFT OBJECTS

We now return to sliding motions discussed in Section 2 and focus on macroscopic objects. This time, we consider situations where the surfaces are pressed into each other under an externally applied normal force N. Now, elastic deformation occurs even in the absence of motion. The solids deform as they make conformal (or Hertzian) solid-solid contact, a classical problem in solid mechanics (Landau & Lifshitz 1986, Johnson 1987). Relative sliding between the surfaces breaks this contact by entraining the surrounding fluid, which establishes a thin intervening fluid film that lubricates the surfaces. This regime of conformal lubricated sliding is a well-studied tribological problem (Dowson & Higginson 1959, Bisset 1989). Although the conformal regime may be analyzed for a prescribed fixed vertical indentation (see, e.g., Weekley et al. 2006, Wu et al. 2023), it is much more common to prescribe the normal load as we do here. The hydrodynamic normal force is then no longer of interest, as it simply balances the applied normal load at steady state. Instead, the typical quantities of interest are now the tangential force (drag) and the film thickness.

4.1. Flow Structure: Thin Films and Boundary Layers

As a canonical example, we consider a rigid spherical indenter that is pushed into a soft material under a prescribed normal force N. In the absence of fluid the sphere indents a depth $d_{p,\mathrm{dry}}$ into the soft solid, establishing solid-solid contact over a circular area that, according to the theory of Hertz, has a radius $a = \sqrt{d_{p,\mathrm{dry}}R} \sim (NR/G)^{1/3}$. If the sphere is now slid relative to the soft material, a thin fluid film is entrained and slightly separates the surfaces, so that the effective indentation depth decreases to a value $d_p \leq d_{p,\mathrm{dry}}$. We thus see that the clearance between the undeformed surfaces (in the sense defined in Section 2) is simply the negative of the indentation depth $d = -d_p$. The regime of sliding speeds with negative clearance d (positive indentation d_p) is that of conformal EHL.

When the film thickness becomes comparable to the dry indentation depth, the normal force due to the lubrication flow in the thin film has the scale $\mu V a^3/d_{p,\mathrm{dry}}^2$, which must balance the applied normal force N at steady state. The ratio of these characteristic force scales identifies a dimensionless quantity

$$\lambda = \frac{\mu V R^{5/3} G^{1/3}}{N^{4/3}}. \qquad 18.$$

The parameter λ is a dimensionless velocity, and in this way it is analogous to the quantity η introduced in Section 2. Unlike η, however, λ is not a compliance but rather a stiffness. This is because the normal force, rather than the vertical penetration depth, is being held constant. For any particular speed λ, the penetration depth is determined self-consistently from the solution of the Reynolds equation by requiring that the applied load is balanced by the hydrodynamic normal force $N = \int p dA$. As λ increases (greater relative speed), the entrained fluid film becomes thicker and the penetration depth d_p varies smoothly from its positive Hertzian value (dry indentation; $d < 0$) to a negative one (nonconformal sliding, positive clearance $d > 0$). The fixed-load analysis thus spans both conformal and nonconformal regimes, with $\lambda \ll 1$ (small speeds or large loads) approaching the dry Hertzian limit, and $\lambda \gg 1$ (large speeds or small loads) approaching the nonconformal small-deformation limit $\eta \ll 1$ of Section 2 (**Figure 5*a***).

For a cylinder pressed into a thick substrate and slid along it (the quantity analogous to λ in Equation 18 is $\lambda_{2D} = \mu VRG/N^2$, where N is now the applied force per length), a matched asymptotic analysis for small speeds finds that the thin film is of approximately uniform thickness over the contact area and scales as $(\mu VR)^{3/5}/(N^{1/5}G^{1/5})$ (Snoeijer et al. 2013). The inlet and outlet to the thin film are characterized by boundary layers (see **Figure 5*b*,*c***) of width $\sqrt{d_p R}\,\lambda_{2D}^{2/5}$. The thickness of the lubricating film is set by the structure of the boundary layer at the entrance (inlet) to the

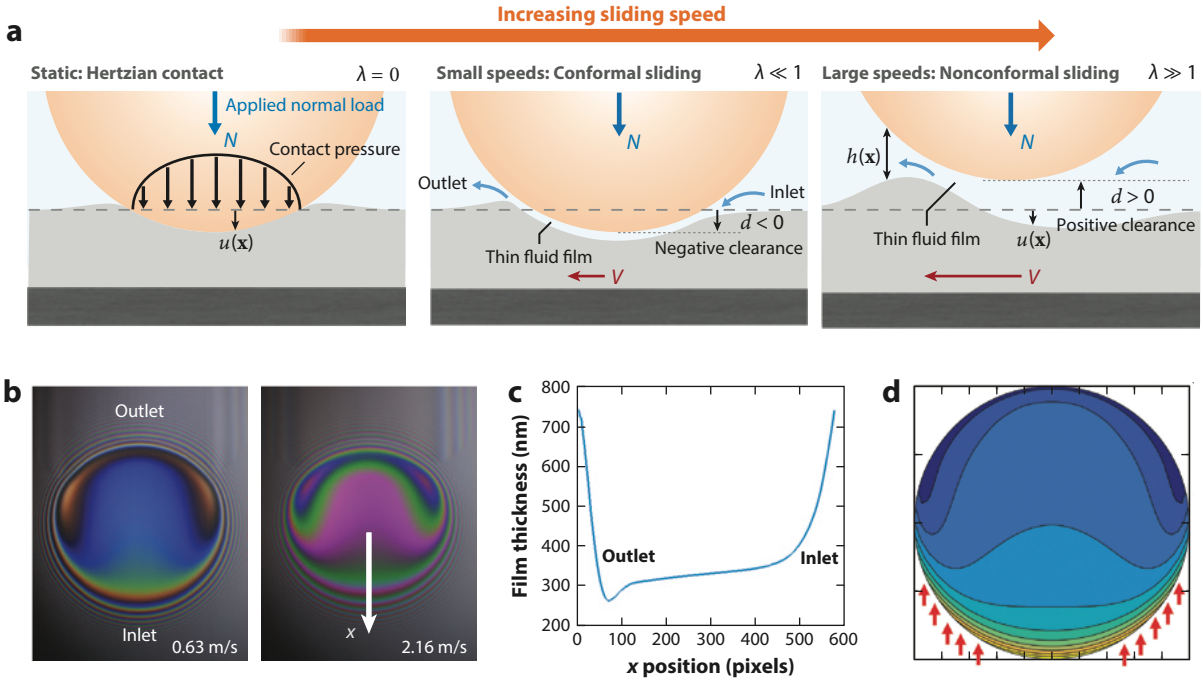

Figure 5

(*a*) Conformal versus nonconformal elastohydrodynamic lubrication. For a fixed normal load, greater sliding speeds support thicker films and allow the object to maintain a greater separation distance from the soft material. When the lubricated film is thinner than the surface displacement, the objects are in near-conformal sliding, whereas when the film is thicker than the deformation, the objects are in nonconformal sliding. (*b*) Optical interferometry measurements of film thickness show rapid variations near the inlet and outlet regions, and a mostly uniform film thickness near the middle of contact. (*c*) A film thickness profile along the direction of motion, obtained using interferometry, resolves features as small as about 100 nm. (*d*) Contours of film thickness, obtained from numerical solutions; arrows indicate the inlet. Panels adapted with permission from (*b*,*c*) Marx et al. (2016) and (*d*) Wu et al. (2020).

NUMERICAL METHODS FOR ELASTOHYDRODYNAMIC LUBRICATION

The solution to elastohydrodynamic lubrication problems between soft materials in conformal contact is numerically challenging for several reasons. The film becomes asymptotically thin, boundary layers develop at the entrance and exit to the thin film, and the dry limit ($\lambda = 0$) has a discontinuous structure. An added complication is the singular kernel of the Green's function relating displacement to pressure. Iterative methods are simple to implement but tend to be very sensitive to initial guesses (for a detailed discussion, see Hui et al. 2021). Recently developed numerical methods use implicit (noniterative) time-dependent formulations to overcome some of these challenges (Liu et al. 2022, Wu et al. 2023), although one must guard against slow transients associated with fluid drainage from thin films. Computational advantage may also be realized by an adaptive collocation of grid points around boundary layers (Singh et al. 2021).

film, a feature that is shared with the motion of long bubbles through tubes (Bretherton 1961). Hui et al. (2021) analyzed the sliding of a cylinder on both elastic and viscoelastic substrates, and developed simple and accurate approximations for the film thickness, pressure distribution, and friction coefficient. For thin compressible layers (thickness $b \ll a \ll R$), the Winkler approximation is not universally applicable for all speeds in the fixed-load analysis, particularly for small speeds when the width of the entrance region becomes comparable to the thickness of the soft layer (Essink et al. 2021). This leads to two different scaling behaviors for the film thickness at small speeds, which in turn controls the drag experienced by the object.

The qualitative features remain unchanged for spherical objects (although a quantitative analysis is much more difficult), and fluid invades the entire region of contact as soon as sliding is initiated (**Figure 5*b***). Detailed experimental measurements of film thickness profiles as small as 100 nm are made possible by interferometry techniques (**Figure 5*c***) (Spikes 1999, Liu et al. 2015, Marx et al. 2016). Numerical solution strategies for spherical geometries are significantly more involved but are tractable (**Figure 5*d***) (see, e.g., Wu et al. 2020; the sidebar titled Numerical Methods for Elastohydrodynamic Lubrication).

4.2. Elastohydrodynamic Torque: Coupling of Rotation and Translation

A less investigated feature of EH sliding is the generation of torques. For nonconformal configurations and small deformations, the torque due to fluid-elastic interactions occurs at quadratic order in deformation and scales as (for a sphere)

$$T^{\mathrm{EH}} \sim \int \eta^2 \frac{\mu V}{d^2} \mathrm{d}A \sim \frac{\mu^3 V^3 R^3 \ell_s^2}{K^2 d^5} \quad \text{(nonconformal contact; sphere).} \qquad 19.$$

During sliding, objects that are free to rotate (zero externally applied torque) will experience an EH contribution to rotation at a rate $\Omega \propto \eta^2 V/R$ (recall that η scales with speed). A detailed analysis confirms this scaling quantitatively for cylinders (Skotheim & Mahadevan 2005, Rallabandi et al. 2017) and spheres (Bertin et al. 2022). For short cylinders of length L_c sliding on an incline, contributions due to end effects produce an additional rotation with angular velocity $(VR^2/L_c)\eta \log \eta$, which recovers experimental measurements at small speeds (Saintyves et al. 2020). However, rotation rates in experiments can reach $R\Omega/V \approx 1$, much greater than predictions of theory for nonconformal contacts, even at large η. Allowing for conformal deformations at fixed normal load resolves this discrepancy and predicts $R\Omega/V \to 1$ in the small λ (large load) limit (Kargar-Estahbanati & Rallabandi 2022). Thus, conformal contact between sliding objects encourages a strong coupling between rotational and sliding motions, leading to pure rolling in

the Hertzian limit. Equally, rotation makes a sizeable contribution to the drag on the object in the conformal regime and is an important consideration in the tribometry of soft materials (de Vicente et al. 2005).

4.3. Lubricated Friction and the Transition to Solid Friction

The role of a lubricating fluid on the frictional properties between a pair of sliding surfaces (a tribopair) is an important aspect of EH lubrication in the conformal regime. The ratio of the hydrodynamic drag force $F_\parallel$ opposing motion to the applied normal load N defines the coefficient of friction $f = F_\parallel / N$. The drag on a lubricated object depends on hydrodynamic stresses and scales as $F_\parallel \sim \mu a^2 V / h^*$, where h^* is a characteristic film thickness. Because h^* scales sublinearly with velocity in the conformal regime, the EHL contribution to the friction increases with sliding speed and vanishes as $V \to 0$ (perhaps counterintuitively, the coefficient of friction between lubricated soft materials is lower for thinner films when the normal load is held fixed). However, in the absence of lubricant, friction is mediated by solid-solid contacts and the coefficient of friction takes on a nonzero static value f_s.

How, then, does one transition from a nonzero coefficient of static friction to the vanishingly small coefficient of lubricated friction at small speeds? This transition between the dry and lubricated regimes of soft sliding contact is referred to as mixed lubrication (see **Figure 6*b***). The mixed regime is presumed to comprise interspersed regions of solid-solid contact and lubricated contact, and is connected to surface roughness features (asperities) that are usually ignored in lubrication theory. Experimental data for hard materials suggest that the mixed regime is relevant when the film thickness is a few times the characteristic asperity size, though recent experiments show that this transition may occur for much thicker films and is associated with the formation of surface wrinkles (Dong et al. 2023).

Descriptions of the mixed lubrication regime typically split the normal load between solid-solid and thin-film contact in a relative proportion that depends on the film thickness (see, e.g., Persson & Scaraggi 2009). While such models qualitatively capture the variation of friction versus sliding speed (the Stribeck curve), the detailed dynamics by which the lubricating fluid film breaks to produce solid contact has been the subject of debate for both rigid and soft geometries (see, e.g., Jamali & Brady 2019, Jamali et al. 2020, Dong et al. 2023). Transients bring soft surfaces temporarily closer to each other than at steady state, but without any finite-time solid contact (Weekley et al. 2006). By contrast, porosity of the objects does allow contact at finite sliding speeds; the critical speed for contact was found to scale with permeability with an exponent of about 0.65 (Zakhari & Bonnecaze 2021). A detailed quantification of the relation between surface roughness, mechanisms of dry friction, and the transition to EH lubricated friction remains a challenging interdisciplinary problem.

4.4. Patterned Surfaces

The interaction of fluid flow and elastic deformation becomes more complex when one or both objects are decorated with surface patterns. Examples occur in sensing and haptics, where the texture is either a part of the soft object (e.g., fingertip asperities) or a surface whose texture is to be sensed. It is well established experimentally that surface patterns strongly influence the properties of the lubricated film (Kaneta & Cameron 1980, Choo et al. 2008) (see **Figure 6*a***). Recent experiments with fingertips sliding on glass substrates have shown that the deformation of fingertip asperities and trapped pockets of air are both involved in sliding friction and that small vibrations can modify these frictional properties (Wiertlewski et al. 2016). In experiments of elastomeric fingers sliding across a soft surface with a ridge pattern, Peng et al. (2021a,b) showed that the coefficient of friction depends nonmonotonically on the sliding speed for textured surfaces

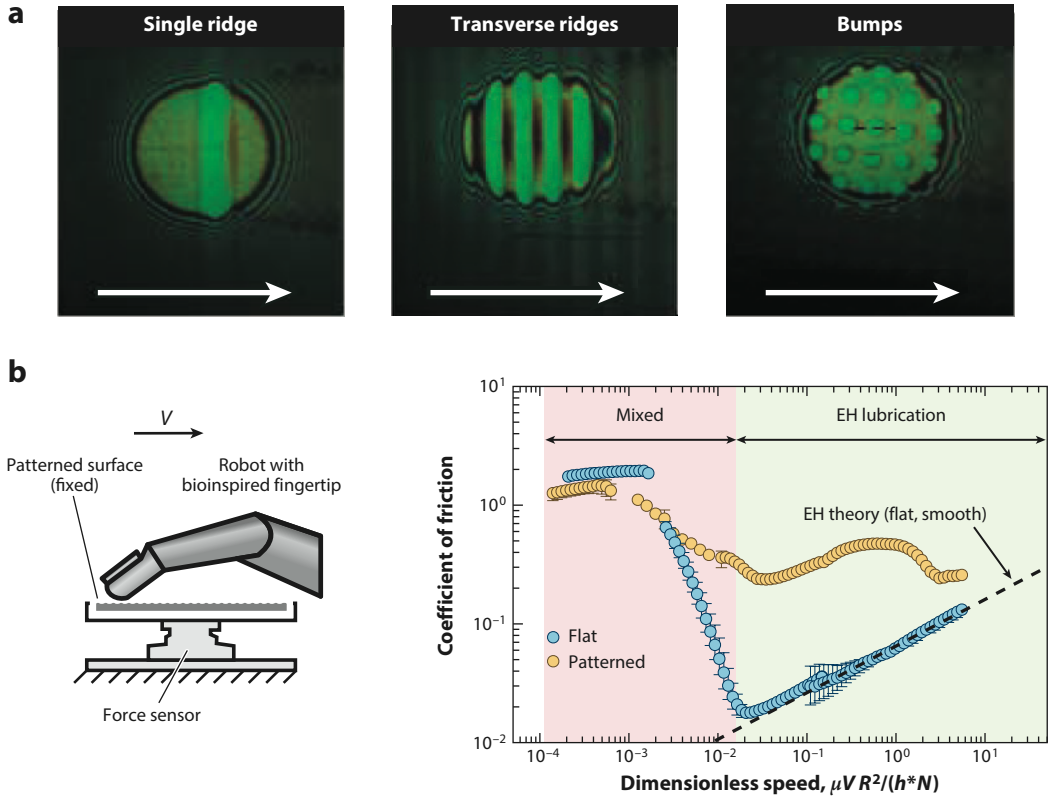

Figure 6

(*a*) Sliding of a soft sphere over various surface patterns. Surface patterns greatly influence the lubricating film, here visualized using interferometry (cf. **Figure 5*b***). (*b*) Sliding a soft finger over a ridge pattern produces a nonmonotonic dependence of the effective coefficient of friction on the sliding speed in the elastohydrodynamic (EH) lubricated regime. This feature is absent for flat (nonpatterned) surfaces. Panels adapted with permission from (*a*) Choo et al. (2008) and (*b*) Peng et al. (2021b).

(**Figure 6*b***). The authors argue that this feature may be due to a crossover of EHL effects from pattern-scale to global scales, possibly compounded by the lateral bending of the ridges.

Theory and simulations of these more complex compliant systems pose several challenges (Zhu & Wang 2011). While the bending response of isolated flexible elements in shear and pressure-driven flow is well understood (Wexler et al. 2013), the response of arrays of such elements is much more complex. Recent theoretical and experimental work has shed some light on such systems (Hosoi 2019). For example, models that treat beds of slender hair-like protrusions on solid substrates as an effective Brinkmann medium (Nasto et al. 2018) or as an impermeable layer with finite bending resistance (Alvarado et al. 2017) have compared favorably with experiments.

5. APPROACH TO CONTACT

The normal approach of soft objects toward contact is important in several contexts including the study of collisions and the dynamics of indentation and adhesion of soft materials. Elastic deformations allow the approaching objects to make contact over a larger area, which in turn leads to greater viscous dissipation. As the intervening fluid film thins to nanometric scales over time, intermolecular forces due to van der Waals or electrostatic interactions can exert significant influence

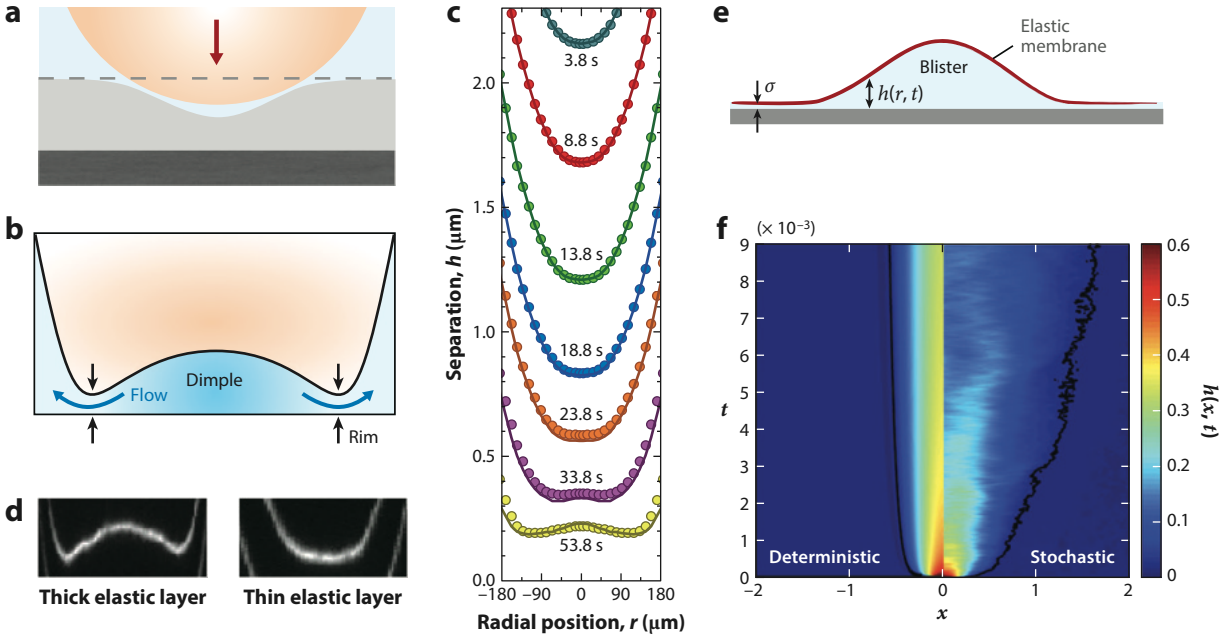

Figure 7

(*a*,*b*) Pushing a soft object into a soft wall produces a dimple that is separated from the outside by a narrow rim. Fluid squeezes out of the dimple as the elastic stresses relax. (*c*) Measurements (*symbols*) and numerical solutions (*curves*) of film thickness during dynamic indentation of a soft polydimethylsiloxane layer with a sphere. (*d*) The dimple may or may not form depending on the thickness and stiffness of the soft layer. (*e*,*f*) A fluid-filled blister under an elastic membrane relaxes slowly due to bending stresses and can be expedited by thermal fluctuations. Panels adapted with permission from (*c*,*d*) Wang et al. (2015) and (*f*) Carlson (2018).

on the dynamics. We discuss this interplay between hydrodynamic, elastic, and intermolecular forces in near-contact configurations here.

5.1. Normal Approach of Solid Objects: Formation and Drainage of Dimples

As soft objects approach each other through viscous fluid, the pressure of the flow is greatest at the point of minimum separation and deforms the objects to create a central dimple (**Figure 7*a*,*b***). The dimple is under high elastic stress and relaxes by squeezing fluid out into the surrounding region. Depending on the compliance of the system, the dimple may relax relatively quickly or may further deepen as the objects approach. In this latter case, the dimple is separated from the outer fluid by a narrow circular rim through which fluid must drain (**Figure 7*b***). The narrowness of the rim combined with the wide contact area under the dimple slows down drainage of the fluid as the surfaces approach contact, producing a much greater viscous resistance than would be expected for rigid objects. Soft objects thus make contact over greater contact areas, and over much longer timescales, than their rigid counterparts.

Davis et al. (1986) modeled the collision and rebound between two soft spheres, accounting for their inertia but neglecting the inertia of the fluid. As the spheres approach each other, there is a substantial flattening of the contact surfaces, leading to either sticking or rebounding. This model was verified experimentally by Barnocky & Davis (1988). More recent work has modeled roughness effects (Scaraggi & Persson 2012), the effect of a thin elastic coating on the rebound problem (Tan et al. 2019), and the effects of fluid compressibility (Balmforth et al. 2010). When

the initial separation d and initial normal velocity $V_\perp$ are prescribed (as in the collision problem), a balance of viscous and elastic stresses once again identifies a dimensionless compliance (for a spherical object) $\mu V_\perp R^{3/2}/(Gd^{5/2})$, though other quantities are usually also relevant depending on the forces acting on the system.

Using an SFA, Wang et al. (2015) made direct measurements of the deformation profiles during the normal approach of a sphere on soft PDMS layers mounted on rigid substrates (**Figure 7*a*,*c***). While dimples were observed for thick layers, the contact region was flat for a thin PDMS layer, which is geometrically stiffer and therefore deforms less and relaxes more quickly (**Figure 7*d***). A more detailed numerical study confirms this argument (Wang et al. 2017). Many of the qualitative features described above are also observed in the impact and settling of droplets on solid surfaces (Snoeijer 2016). Poulain & Carlson (2022) recently studied a version of the problem involving a droplet settling on a soft surface, where the drainage dynamics are slowed even further due to the combined elastic and capillary deformations.

5.2. Drainage of Fluid-Filled Blisters

The drainage of fluid due to elastic stresses is not restricted to the contact dynamics of compact objects. A related system that shares some of the features of contacting elastic solids is the closing of fluid-filled blisters between elastic membranes and rigid surfaces (**Figure 7*e***). Once again, the problem may be studied using the thin-film equation, where now the pressure is related to the bending deformation of the sheet according to $p = B\nabla^4 h$ (neglecting stretching effects and the weight of the sheet). The height of the thin film evolves according to (Michaut 2011, Lister et al. 2013)

$$\frac{\partial h}{\partial t} = \frac{B}{12\mu}\nabla \cdot \left(h^3 \nabla \left(\nabla^4 h\right)\right). \qquad 20.$$

The bending rigidity of the sheet drives it to make contact with the rigid substrate by squeezing fluid out of the blister. This causes the blister to spread out over time as the elastic membrane flattens. It is typical to assume a prewetted film of a molecularly small thickness σ to tame moving contact line singularities of the thin film equation. As the sheet approaches its fully relaxed state $h \sim \sigma$, the dynamics become linear and self-similar. Scaling estimates and detailed analysis of Equation 20 in this limit (Pedersen et al. 2021) find that the radius of the blister grows as $t^{1/6}$, and its height decreases as $t^{-1/3}$ to conserve volume. Thermal fluctuations of the fluid speed up the dynamics significantly (both the prefactor and the power law exponent) when they dominate over bending (Carlson 2018, Pedersen et al. 2019) (see **Figure 7*f***).

5.3. The Role of Intermolecular Forces

When the separation distance between approaching objects is on the order of a few nanometers, intermolecular forces may play an important role, either aiding or preventing contact. The role of intermolecular forces is further enhanced in soft systems, where compliance of the boundaries allows for close conformal contact over a relatively large surface area. While static adhesive contact of soft materials is well understood through classical theories of adhesion (Johnson 1987) and more recent work (Style et al. 2017), the fluid dynamics leading up to adhesion have received less attention.

Van der Waals and electrostatic interactions are common sources of intermolecular forces and, when attractive, can cause nearby surfaces to approach and eventually adhere (making conformal contact). This process may be made nontrivial when the bodies must move through fluid to make contact. Sun et al. (2021) experimentally examined the role of adhesion forces between submerged soft PDMS layers and functionalized glass surfaces. Using frustrated total internal

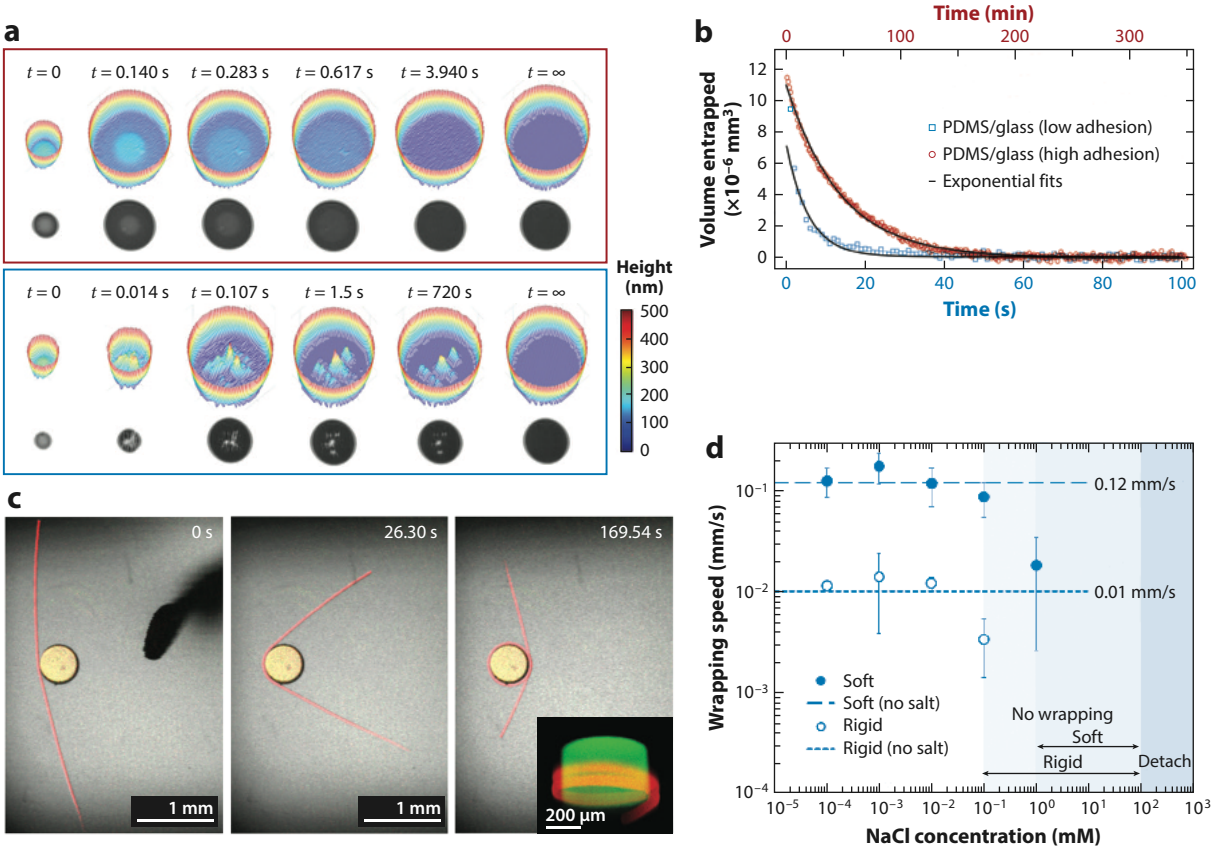

Figure 8

(*a*) Height maps show the formation of contact between a submerged polydimethylsiloxane (PDMS) lens and a surface-treated glass substrate with lower (*top*) and higher (*bottom*) adhesive energies. (*b*) Entrapped liquid drains much more slowly when the adhesive energy is higher. Red and blue plots correspond to red and blue axes, respectively. (*c*) A charged fiber wraps around an oppositely charged particle. (*d*) Softer fibers wrap more quickly. Panels adapted with permission from (*a*,*b*) Sun et al. (2021) and (*c*,*d*) Nunes et al. (2021).

reflection microscopy, they made the counterintuitive observation that a modest increase in adhesion energy (assessed by contact angle measurements) greatly prolongs the time to make complete contact (**Figure 8*a*,*b***). The authors explain these observations by noting that adhesive forces drive the rim to close first, which effectively traps liquid in the dimple. In another experimental study, Nunes et al. (2021) observed the wrapping of charged fibers around oppositely charged soft particles (**Figure 8*c***). They found that the rate of wrapping is faster for softer particles (**Figure 8*d***) and is independent of the free length of the fiber, and hypothesized that the wrapping dynamics is controlled locally by elastohydrodynamics of adhesive contact.

The effect of intermolecular forces is typically modeled as a disjoining (or adhesive) pressure $\Pi_d(h) = -\mathrm{d}\Phi/\mathrm{d}h$, where $\Phi(h)$ is an interaction potential with units of energy per area. A typical interaction potential that includes a long-range van der Waals attraction and a short-range repulsion is (Israelachvili 2011)

$$\Phi(h) = -\frac{A}{6\pi}\left(\frac{1}{2h^2} - \frac{\sigma^6}{8h^8}\right) \Rightarrow \Pi_d(h) = \frac{A}{6\pi h^3}\left(1 - \frac{\sigma^6}{h^6}\right). \qquad 21.$$

Here, A is a Hamaker constant (positive for attractive interactions, typically about 10^{-19} J), and σ is the equilibrium separation distance of the potential (usually taken to be about 1 Å). Electrostatic potentials are conceptually similar but are typically screened by ions in the fluid over nanometric scales and are sometimes combined with van der Waals potentials in DLVO (Derjaguin–Landau–Verwey–Overbeek) theory (Israelachvili 2011). The pressure of the flow is then counteracted by a superposition of an elastic normal stress and the disjoining pressure.

The adhesive contact of thin elastic membranes has received some theoretical attention. Now, the pressure of the fluid is counteracted by a combination of a bending stress and an intermolecular stress, so $p = B\nabla^4 h + \Pi_d$. Carlson & Mahadevan (2016) analyzed the contact dynamics of a thin elastic sheet onto a surface due to an attractive van der Waals potential and showed that the gap closes as $h \propto (t_c - t)^{1/3}$ (t_c is the time at which the gap fully closes) and the sheet has a self-similar shape over a length scale $\propto (t_c - t)^{1/3}$ in the approach to contact (cf. **Figure 7*e***). Other work has analyzed the propagation of adhesive and peeling fronts in dynamic, directional adhesion of elastic sheets due to van der Waals forces (Poulain et al. 2022).

We return once more to the nonconformal motion of particles near soft substrates, and this time briefly discuss the role of intermolecular forces. Assuming small deformations, Urzay (2010) analyzed the role of DLVO interactions on the motion of a sphere near a soft wall, predicting both reversible and irreversible adhesion behaviors. More recently, Karan et al. (2020, 2021) studied the effect of these interactions on time-dependent normal motion in a similar configuration. In addition to deformation due to flow, van der Waals pressure produces elastic deformations of magnitude $AR^{1/2}/(Gd^{5/2})$ [note that d is clearance between the surfaces (see Section 2)], which defines another dimensionless compliance $AR^{1/2}/(Gd^{7/2})$. The inclusion of electrostatic interactions adds yet another compliance parameter, which depends sensitively on the separation relative to the Debye screening length. Particle motion is now governed by a three-way interplay between elastic, hydrodynamic, and intermolecular stresses, each of which influences (and is influenced by) the geometry of the fluid film. This interplay can lead to far greater forces than would be expected from a superposition of the individual contributions.

6. CONNECTIONS WITH OTHER DEFORMABLE SYSTEMS IN FLOW

The bulk of this review has focused on soft compact objects close to contact and the various phenomena and interactions that may arise due to an interplay between fluid flow and elastic deformation. Fluid-elastic interactions are important in many other types of systems that this review does not have the room to discuss in detail. Here we point out some connections of the present discussion with these systems.

6.1. Deformable Particles

Red blood cells flowing in narrow capillaries tend to preferentially flow near the centerline, establishing a depleted cell-free region near the walls of the capillary. Early work by Secomb et al. (1986) modeled the pressure-driven motion of a vesicle in a tube and found, assuming constant membrane tension, the thickness of the gap scales as $(\mu V/T)^{2/3}$, analogous to the result of Bretherton (1961) for bubbles in tubes. Savin et al. (2016) performed experiments with single red blood cells flowing in narrow tubes to confirm this scaling law at small velocities but found a transition to a $(\mu V/T)^{1/3}$ power law at larger speeds. Asymptotic and boundary element analysis of vesicles flowing in tubes, accounting for both bending and nonhomogeneous membrane tension (Barakat & Shaqfeh 2018a,b), has found good agreement with experiments. In the last decade, detailed simulations of blood flow have quantified the relationships between cell properties and flow in capillaries (Kumar & Graham 2012, Freund 2014, Bächer et al. 2017). Several aspects of the flow of vesicles, deformable cells, and capsules are discussed in the review by Barthès-Biesel

(2016). Deformation of particles has also been implicated in the shear-thickening rheology of dense suspensions. Many models have directly used the static contact theory of Hertz to estimate deformation and have yielded excellent agreement with rheological measurements (see, e.g., Bonnecaze & Cloitre 2010, Seth et al. 2011, Bonnecaze et al. 2020).

6.2. Particles in Compliant Channels

There has also been growing interest in flows through compliant channels and conduits. The recent review by Christov (2022) discusses flow through compliant channels, including nonlinear pressure-flux relations, analytical approximations, and applications. Some of this work has focused on particulate flows and has considered the motion of both undersized (Tözeren & Skalak 1978, Takagi & Balmforth 2011) and oversized objects (Lighthill 1968, Tani et al. 2017, Vurgaft et al. 2019, Rallabandi et al. 2021) in compliant tubes. The qualitative features are remarkably similar to those observed for the sliding of objects near soft substrates discussed in Sections 2 and 4. The pressure of the flow produces a local circumferential stretching of a compliant tube, which in turn leads to radial hoop stress. Rather conveniently, this results in Winkler-like pressure-deformation relations for thin-walled tubes and small deformations, plus additional contributions involving bending and stretching of the tube walls.

6.3. Microswimming near Fluid and Elastic Interfaces

In Section 2 we discussed the motion of passive particles near compliant surfaces, driven either by the application of a force or by a carrying flow. A smaller literature has focused the effect of compliant boundaries on nearby active particles and microswimmers. Deformation of a nearby air-water interface (resisted by interfacial tension) has been shown theoretically to produce a variety of effects including a rectification of periodic motion (Trouilloud et al. 2008, Crowdy et al. 2011, Dias & Powers 2013, Grosjean et al. 2018) and complex trajectories including attraction to the interface for slender swimmers (Nambiar & Wettlaufer 2022). In the context of elastic boundaries, Ledesma-Aguilar & Yeomans (2013) showed that the flexibility of confining boundaries enhances the motility of pusher- and puller-type swimmers. The same qualitative conclusion was drawn by Dalal et al. (2020), who performed boundary element simulations of ameboid swimming in a compliant channel. Self-propelled objects differ from the passive particles discussed thus far in that they typically experience no hydrodynamic force, so their leading hydrodynamic singularity is a force dipole. These singularities have a different spatial structure than for externally forced particle motion, and the flows they generate decay more rapidly with distance from the swimmer. For this reason, the role of interfacial deformations is likely to be most relevant when the distance to the surface is comparable to (or smaller than) the size of the swimmer.

6.4. Slender Flexible Filaments

There is a well-developed literature on the deformation of slender flexible filaments interacting with fluid flow that we have largely left untouched (see the reviews by du Roure et al. 2019 and Duprat 2022). It is common to analyze the deformation of these objects using elastica theory and the fluid flow they generate using slender body hydrodynamics, which is a significant departure from the theoretical ideas discussed here. A growing body of work has also applied the hydrodynamics of flexible filaments to analyze motility and feeding mechanisms of microorganisms, including a coupling to the binding kinetics of molecular motors, as well as mechanisms of synchronization between multiple cilia/flagella through hydrodynamic, elastic, and molecular signaling mechanisms. These topics present several experimental and theoretical challenges in fluid and solid biomechanics at submicron scales but are beyond the focus of this review.

7. CONCLUSIONS

Interactions between moving objects, deformable surfaces, and fluid flow are important in a wide range of systems and are a rich source of problems, as we have hopefully conveyed. Such interactions are often strongest when objects are in proximity with one another, producing flow phenomena that are tightly coupled to elastic deformation. These effects may be exploited to manipulate particle trajectories in channels, to probe the mechanical properties of soft materials without direct solid-solid contact, or for grasping and sensing applications in robotics. Theoretical and modeling approaches are relatively well-developed and have relied on EHL theory. When the objects are in very close contact, features such as surface roughness and intermolecular forces may have a significant effect on the kinematics and dynamics of the fluid-elastic interactions.

Recent experiments have demonstrated that EH lubrication effects are not restricted to macroscopic settings but are also important in microscale flows. There is a need to further develop careful experiments and theory to probe and quantify these microscale EH interactions, both in engineered flows and in biophysical systems. Simultaneous measurements of forces combined with visualization of deformations would advance the field and are likely to spur new ideas. Understanding the effects of complex geometries on EH interactions, such as naturally occurring surface asperities or engineered surface textures, is another promising direction for exploration. Equally, quantifying the role of intermolecular forces, and the effects of using materials with nonlinear or nonhomogeneous material properties, is bound to present new challenges and opportunities for experiment, computation, and theory.

SUMMARY POINTS

1. Interactions between viscous fluid flow and soft structures arise in a wide range of contexts including rheology, tribology, and biology.
2. Suspended objects moving near soft boundaries may experience additional forces or torques and modified kinematics that depend on elastic properties.
3. An interplay of elastic, viscous, and intermolecular forces along with complex geometrical features can significantly influence the dynamics of soft objects near contact.

DISCLOSURE STATEMENT

The author is not aware of any biases that might be perceived as affecting the objectivity of this review.

ACKNOWLEDGMENTS

I am indebted to many colleagues and collaborators for discussions on topics relevant to this article. In particular, I thank A. Kargar-Estahbanati, N. Oppenheimer, T. Salez, and H.A. Stone for feedback on an early draft of this article. I thank the National Science Foundation for partial support.

LITERATURE CITED

Abkarian M, Lartigue C, Viallat A. 2002. Tank treading and unbinding of deformable vesicles in shear flow: determination of the lift force. *Phys. Rev. Lett.* 88:068103

Alvarado J, Comtet J, de Langre E, Hosoi AE. 2017. Nonlinear flow response of soft hair beds. *Nat. Phys.* 13:1014–19

Archard G, Gair F, Hirst W. 1961. The elasto-hydrodynamic lubrication of rollers. *Proc. R. Soc. A* 262:51–72
Bächer C, Schrack L, Gekle S. 2017. Clustering of microscopic particles in constricted blood flow. *Phys. Rev. Fluids* 2:013102
Balmforth NJ, Cawthorn CJ, Craster RV. 2010. Contact in a viscous fluid. Part 2. A compressible fluid and an elastic solid. *J. Fluid Mech.* 646:339–61
Barakat JM, Shaqfeh ESG. 2018a. The steady motion of a closely fitting vesicle in a tube. *J. Fluid Mech.* 835:721–61
Barakat JM, Shaqfeh ESG. 2018b. Stokes flow of vesicles in a circular tube. *J. Fluid Mech.* 851:606–35
Barnocky G, Davis RH. 1988. Elastohydrodynamic collision and rebound of spheres: experimental verification. *Phys. Fluids* 31:1324–29
Barthès-Biesel D. 2016. Motion and deformation of elastic capsules and vesicles in flow. *Annu. Rev. Fluid Mech.* 48:25–52
Beaucourt J, Biben T, Misbah C. 2004. Optimal lift force on vesicles near a compressible substrate. *Europhys. Lett.* 67:676–82
Berdan C, Leal LG. 1982. Motion of a sphere in the presence of a deformable interface: I. Perturbation of the interface from flat: the effects on drag and torque. *J. Colloid Interface Sci.* 87:62–80
Bertin V, Amarouchene Y, Raphael E, Salez T. 2022. Soft-lubrication interactions between a rigid sphere and an elastic wall. *J. Fluid Mech.* 933:A23
Bertin V, Zhang Z, Boisgard R, Grauby-Heywang C, Raphaël E, et al. 2021. Contactless rheology of finite-size air-water interfaces. *Phys. Rev. Res.* 3:L032007
Bickel T. 2006. Brownian motion near a liquid-like membrane. *Eur. Phys. J. E* 20:379–85
Bickel T. 2007. Hindered mobility of a particle near a soft interface. *Phys. Rev. E* 75:041403
Bisset EJ. 1989. The line contact problem of elastohydrodynamic lubrication – I. Asymptotic structure for low speeds. *Proc. R. Soc. A* 424:393–407
Boatwright T, Dennin M, Shlomovitz R, Evans AA, Levine AJ. 2014. Probing interfacial dynamics and mechanics using submerged particle microrheology. II. Experiment. *Phys. Fluids* 26:071904
Bonnecaze RT, Cloitre M. 2010. Micromechanics of soft particle glasses. In *High Solid Dispersions*, ed. M Cloitre, pp. 117–61. Berlin: Springer
Bonnecaze RT, Khabaz F, Mohan L, Cloitre M. 2020. Excess entropy scaling for soft particle glasses. *J. Rheol.* 64:423–31
Brenner H. 1961. The slow motion of a sphere through a viscous fluid towards a plane surface. *Chem. Eng. Sci.* 16:242–51
Bretherton FP. 1961. The motion of long bubbles in tubes. *J. Fluid Mech.* 10:166–88
Brochard F, Lennon J. 1975. Frequency spectrum of the flicker phenomenon in erythrocytes. *J. Phys.* 36:1035–47
Bureau L, Coupier G, Salez T. 2023. Lift at low Reynolds number. *Eur. Phys. J.* 46(11):1–43
Carlson A. 2018. Fluctuation assisted spreading of a fluid filled elastic blister. *J. Fluid Mech.* 846:1076–87
Carlson A, Mahadevan L. 2016. Similarity and singularity in adhesive elastohydrodynamic touchdown. *Phys. Fluids* 28:011702
Chan PH, Leal L. 1979. The motion of a deformable drop in a second-order fluid. *J. Fluid Mech.* 92:131–70
Chandler TGJ, Vella D. 2020. Validity of Winkler's mattress model for thin elastomeric layers: beyond Poisson's ratio. *Proc. R. Soc. A* 476:20200551
Choo JW, Olver AV, Spikes HA, Dumont ML, Ioannides E. 2008. Interaction of asperities on opposing surfaces in thin film, mixed elastohydrodynamic lubrication. *J. Tribol.* 130:021505
Christov IC. 2022. Soft hydraulics: from Newtonian to complex fluid flows through compliant conduits. *J. Phys. Condens. Matter* 34:063001
Coyle DJ. 1988. Forward roll coating with deformable rolls: a simple one-dimensional elastohydrodynamic model. *Chem. Eng. Sci.* 43:2673–84
Crook AW. 1961. Elastohydrodynamic lubrication of rollers. *Nature* 190:1182–83
Crowdy D, Lee S, Samson O, Lauga E, Hosoi AE. 2011. A two-dimensional model of low-Reynolds number swimming beneath a free surface. *J. Fluid Mech.* 681:24–47
Daddi-Moussa-Ider A, Gekle S. 2016. Hydrodynamic interaction between particles near elastic interfaces. *J. Chem. Phys.* 145:014905

Daddi-Moussa-Ider A, Guckenberger A, Gekle S. 2016. Long-lived anomalous thermal diffusion induced by elastic cell membranes on nearby particles. *Phys. Rev. E* 93:012612
Daddi-Moussa-Ider A, Lisicki M, Gekle S. 2017. Mobility of an axisymmetric particle near an elastic interface. *J. Fluid Mech.* 811:210–33
Daddi-Moussa-Ider A, Rallabandi B, Gekle S, Stone HA. 2018. Reciprocal theorem for the prediction of the normal force induced on a particle translating parallel to an elastic membrane. *Phys. Rev. Fluids* 3:084101
Dalal S, Farutin A, Misbah C. 2020. Amoeboid swimming in a compliant channel. *Soft Matter* 16:1599–613
Davies HS, Débarre D, El Amri N, Verdier C, Richter RP, Bureau L. 2018. Elastohydrodynamic lift at a soft wall. *Phys. Rev. Lett.* 120:198001
Davis RH, Serayssol JM, Hinch EJ. 1986. The elastohydrodynamic collision of two spheres. *J. Fluid Mech.* 163:479–97
de Vicente J, Stokes J, Spikes H. 2005. The frictional properties of Newtonian fluids in rolling–sliding soft-EHL contact. *Tribol. Lett.* 20:273–86
Dias MA, Powers TR. 2013. Swimming near deformable membranes at low Reynolds number. *Phys. Fluids* 25:101901
Dillard DA, Mukherjee B, Karnal P, Batra RC, Frechette J. 2018. A review of Winkler's foundation and its profound influence on adhesion and soft matter applications. *Soft Matter* 14:3669–83
Dong H, Moyle N, Wu H, Khripin CY, Hui CY, Jagota A. 2023. Transition from elastohydrodynamic to mixed regimes in lubricated friction of soft solid surfaces. *Adv. Mater.* 35(17):2211044
Dowson D, Higginson GR. 1959. A numerical solution to the elasto-hydrodynamic problem. *J. Mech. Eng. Sci.* 1:6–15
du Roure O, Lindner A, Nazockdast EN, Shelley MJ. 2019. Dynamics of flexible fibers in viscous flows and fluids. *Annu. Rev. Fluid Mech.* 51:539–72
Duprat C. 2022. Moisture in textiles. *Annu. Rev. Fluid Mech.* 54:443–67
Essink MH, Pandey A, Karpitschka S, Venner CH, Snoeijer JH. 2021. Regimes of soft lubrication. *J. Fluid Mech.* 915:A49
Ewoldt RH, Saengow C. 2022. Designing complex fluids. *Annu. Rev. Fluid Mech.* 54:413–41
Fitz-Gerald JM. 1969. Mechanics of red-cell motion through very narrow capillaries. *Proc. R. Soc. B* 174:193–227
Fradin C, Abu-Arish A, Granek R, Elbaum M. 2003. Fluorescence correlation spectroscopy close to a fluctuating membrane. *Biophys. J.* 84:2005–20
Freund JB. 2014. Numerical simulation of flowing blood cells. *Annu. Rev. Fluid Mech.* 46:67–95
Greenwood JA. 2020. Elastohydrodynamic lubrication. *Lubricants* 8:51
Grosjean G, Hubert M, Collard Y, Pillitteri S, Vandewalle N. 2018. Surface swimmers, harnessing the interface to self-propel. *Eur. Phys. J. E* 41:137
Guan D, Barraud C, Charlaix E, Tong P. 2017a. Noncontact viscoelastic measurement of polymer thin films in a liquid medium using long-needle atomic force microscopy. *Langmuir* 33:1385–90
Guan D, Charlaix E, Qi RZ, Tong P. 2017b. Noncontact viscoelastic imaging of living cells using a long-needle atomic force microscope with dual-frequency modulation. *Phys. Rev. Appl.* 8:044010
Helfrich W. 1973. Elastic properties of lipid bilayers: theory and possible experiments. *Z. Naturforsch. C* 28:693–703
Hinch EJ. 1972. Note on the symmetries of certain material tensors for a particle in Stokes flow. *J. Fluid Mech.* 54:423–25
Hosoi AE. 2019. Corrsin lecture on hairy hydrodynamics. *Phys. Rev. Fluids* 4:110508
Hu S, Meng F, Doi M. 2023. Effect of fluid viscoelasticity, shear stress, and interface tension on the lift force in lubricated contacts. *J. Chem. Phys.* 159:164106
Hui CY, Wu H, Jagota A, Khripin C. 2021. Friction force during lubricated steady sliding of a rigid cylinder on a viscoelastic substrate. *Tribol. Lett.* 69:30
Israelachvili JN. 2011. *Intermolecular and Surface Forces*. Burlington, MA: Academic
Jamali S, Brady JF. 2019. Alternative frictional model for discontinuous shear thickening of dense suspensions: hydrodynamics. *Phys. Rev. Lett.* 123:138002
Jamali S, Del Gado E, Morris JF. 2020. Rheology discussions: the physics of dense suspensions. *J. Rheol.* 64:1501–24

Johnson KL. 1987. *Contact Mechanics*. Cambridge, UK: Cambridge Univ. Press
Kaneta M, Cameron A. 1980. Effects of asperities in elastohydrodynamic lubrication. *J. Lubricat. Technol.* 102:374–78
Karan P, Chakraborty J, Chakraborty S. 2020. Influence of non-hydrodynamic forces on the elastic response of an ultra-thin soft coating under fluid-mediated dynamic loading. *Phys. Fluids* 32:022002
Karan P, Chakraborty J, Chakraborty S. 2021. Generalization of elastohydrodynamic interactions between a rigid sphere and a nearby soft wall. *J. Fluid Mech.* 923:A32
Kargar-Estahbanati A, Rallabandi B. 2021. Lift forces on three-dimensional elastic and viscoelastic lubricated contacts. *Phys. Rev. Fluids* 6:034003
Kargar-Estahbanati A, Rallabandi B. 2022. Rotation–translation coupling of soft objects in lubricated contact. *Soft Matter* 18:4887–96
Kim S, Karrila SJ. 2013. *Microhydrodynamics: Principles and Selected Applications*. Mineola, NY: Dover
Kimura Y, Mori T, Yamamoto A, Mizuno D. 2005. Hierarchical transport of nanoparticles in a lyotropic lamellar phase. *J. Phys. Condens. Matter* 17:S2937
Kopecz-Muller C, Bertin V, Raphael E, McGraw JD, Salez T. 2023. Mechanical response of a thick poroelastic gel in contactless colloidal-probe rheology. *Proc. R. Soc. A* 479(2271):20220832
Kumar A, Graham MD. 2012. Mechanism of margination in confined flows of blood and other multicomponent suspensions. *Phys. Rev. Lett.* 109:108102
Landau LD, Lifshitz EM. 1986. *Theory of Elasticity*, Vol. 7. New York: Elsevier
Ledesma-Aguilar R, Yeomans JM. 2013. Enhanced motility of a microswimmer in rigid and elastic confinement. *Phys. Rev. Lett.* 111:138101
Leroy S, Charlaix E. 2011. Hydrodynamic interactions for the measurement of thin film elastic properties. *J. Fluid Mech.* 674:389–407
Leroy S, Steinberger A, Cottin-Bizonne C, Restagno F, Léger L, Charlaix É. 2012. Hydrodynamic interaction between a spherical particle and an elastic surface: a gentle probe for soft thin films. *Phys. Rev. Lett.* 108:264501
Li J, Chou TW. 1997. Elastic field of a thin-film/substrate system under an axisymmetric loading. *Int. J. Solids Struct.* 34:4463–78
Lighthill MJ. 1968. Pressure-forcing of tightly fitting pellets along fluid-filled elastic tubes. *J. Fluid Mech.* 34:113–43
Lister JR, Peng GG, Neufeld JA. 2013. Viscous control of peeling an elastic sheet by bending and pulling. *Phys. Rev. Lett.* 111:154501
Liu HC, Guo F, Guo L, Wong PL. 2015. A dichromatic interference intensity modulation approach to measurement of lubricating film thickness. *Tribol. Lett.* 58:15
Liu Z, Dong H, Jagota A, Hui CY. 2022. Lubricated soft normal elastic contact of a sphere: a new numerical method and experiment. *Soft Matter* 18:1219–27
Maali A, Boisgard R, Chraibi H, Zhang Z, Kellay H, Würger A. 2017. Viscoelastic drag forces and crossover from no-slip to slip boundary conditions for flow near air-water interfaces. *Phys. Rev. Lett.* 118:084501
Manikantan H, Squires TM. 2020. Surfactant dynamics: hidden variables controlling fluid flows. *J. Fluid Mech.* 892:P1
Marx N, Guegan J, Spikes HA. 2016. Elastohydrodynamic film thickness of soft EHL contacts using optical interferometry. *Tribol. Int.* 99:267–77
Masoud H, Stone HA. 2019. The reciprocal theorem in fluid dynamics and transport phenomena. *J. Fluid Mech.* 879:P1
Michaut C. 2011. Dynamics of magmatic intrusions in the upper crust: theory and applications to laccoliths on Earth and the Moon. *J. Geophys. Res.* 116(B5):B05205
Nambiar S, Wettlaufer JS. 2022. Hydrodynamics of slender swimmers near deformable interfaces. *Phys. Rev. Fluids* 7:054001
Nasto A, Brun PT, Hosoi AE. 2018. Viscous entrainment on hairy surfaces. *Phys. Rev. Fluids* 3:024002
Nunes JK, Li J, Griffiths IM, Rallabandi B, Man J, Stone HA. 2021. Electrostatic wrapping of a microfiber around a curved particle. *Soft Matter* 17:3609–18
O'Sullivan TC, King RB. 1988. Sliding contact stress field due to a spherical indenter on a layered elastic half-space. *J. Tribol.* 110:235–40

Pandey A, Karpitschka S, Venner CH, Snoeijer JH. 2016. Lubrication of soft viscoelastic solids. *J. Fluid Mech.* 799:433–47

Pedersen C, Niven JF, Salez T, Dalnoki-Veress K, Carlson A. 2019. Asymptotic regimes in elastohydrodynamic and stochastic leveling on a viscous film. *Phys. Rev. Fluids* 4:124003

Pedersen C, Salez T, Carlson A. 2021. Universal self-similar attractor in the bending-driven levelling of thin viscous films. *Proc. R. Soc. A* 477:20210354

Peng Y, Serfass CM, Hill CN, Hsiao LC. 2021a. Bending of soft micropatterns in elastohydrodynamic lubrication tribology. *Exp. Mech.* 61:969–79

Peng Y, Serfass CM, Kawazoe A, Shao Y, Gutierrez K, et al. 2021b. Elastohydrodynamic friction of robotic and human fingers on soft micropatterned substrates. *Nat. Mater.* 20:1707–11

Persson BNJ, Scaraggi M. 2009. On the transition from boundary lubrication to hydrodynamic lubrication in soft contacts. *J. Phys. Condens. Matter* 21:185002

Poulain S, Carlson A. 2022. Droplet settling on solids coated with a soft layer. *J. Fluid Mech.* 934:A25

Poulain S, Carlson A, Mandre S, Mahadevan L. 2022. Elastohydrodynamics of contact in adherent sheets. *J. Fluid Mech.* 947:A16

Rallabandi B, Eggers J, Herrada MA, Stone HA. 2021. Motion of a tightly fitting axisymmetric object through a lubricated elastic tube. *J. Fluid Mech.* 926:A27

Rallabandi B, Oppenheimer N, Zion MBZ, Stone HA. 2018. Membrane-induced hydroelastic migration of a particle surfing its own wave. *Nat. Phys.* 14:1211–15

Rallabandi B, Saintyves B, Jules T, Salez T, Schönecker C, et al. 2017. Rotation of an immersed cylinder sliding near a thin elastic coating. *Phys. Rev. Fluids* 2:074102

Ramaswamy S, Prost J, Lubensky TC. 1994. Non-linear effects of membrane fluctuations in the dilute lamellar phase. *Europhys. Lett.* 27:285–90

Reynolds O. 1886. IV. On the theory of lubrication and its application to Mr. Beauchamp Tower's experiments, including an experimental determination of the viscosity of olive oil. *Philos. Trans. R. Soc.* 177:157–234

Saintyves B, Jules T, Salez T, Mahadevan L. 2016. Self-sustained lift and low friction via soft lubrication. *PNAS* 113:5847–49

Saintyves B, Rallabandi B, Jules T, Ault J, Salez T, et al. 2020. Rotation of a submerged finite cylinder moving down a soft incline. *Soft Matter* 16:4000–7

Salez T, Mahadevan L. 2015. Elastohydrodynamics of a sliding, spinning and sedimenting cylinder near a soft wall. *J. Fluid Mech.* 779:181–96

Savin T, Bandi MM, Mahadevan L. 2016. Pressure-driven occlusive flow of a confined red blood cell. *Soft Matter* 12:562–73

Scaraggi M, Persson BNJ. 2012. Time-dependent fluid squeeze-out between soft elastic solids with randomly rough surfaces. *Tribol. Lett.* 47:409–16

Secomb TW, Skalak R, Özkaya N, Gross JF. 1986. Flow of axisymmetric red blood cells in narrow capillaries. *J. Fluid Mech.* 163:405–23

Sekimoto K, Leibler L. 1993. A mechanism for shear thickening of polymer-bearing surfaces: elastohydrodynamic coupling. *Europhys. Lett.* 23:113–17

Seth JR, Mohan L, Locatelli-Champagne C, Cloitre M, Bonnecaze RT. 2011. A micromechanical model to predict the flow of soft particle glasses. *Nat. Mater.* 10:838–43

Shlomovitz R, Evans AA, Boatwright T, Dennin M, Levine AJ. 2013. Measurement of monolayer viscosity using noncontact microrheology. *Phys. Rev. Lett.* 110:137802

Singh K, Sadeghi F, Russell T, Lorenz SJ, Peterson W, et al. 2021. Fluid–structure interaction modeling of elastohydrodynamically lubricated line contacts. *J. Tribol.* 143:091602

Skalak R, Tozeren A, Zarda RP, Chien S. 1973. Strain energy function of red blood cell membranes. *Biophys. J.* 13:245–64

Skotheim JM, Mahadevan L. 2004. Soft lubrication. *Phys. Rev. Lett.* 92:245509

Skotheim JM, Mahadevan L. 2005. Soft lubrication: the elastohydrodynamics of nonconforming and conforming contacts. *Phys. Fluids* 17:092101

Smart JR, Leighton DT. 1991. Measurement of the drift of a droplet due to the presence of a plane. *Phys. Fluids A Fluid Dyn.* 3:21–28

Snoeijer JH. 2016. Analogies between elastic and capillary interfaces. *Phys. Rev. Fluids* 1:060506
Snoeijer JH, Eggers J, Venner CH. 2013. Similarity theory of lubricated Hertzian contacts. *Phys. Fluids* 25:101705
Spikes HA. 1999. Thin films in elastohydrodynamic lubrication: the contribution of experiment. *Proc. Inst. Mech. Eng. J* 213:335–52
Stone H, Abkarian M, Bonnecaze R. 2004. *The normal force in sliding lubrication of deformable spheres and substrates*. Abstract for the 57th Annual Meeting of the Division of Fluid Dynamics of the American Physical Society, Seattle, WA, Nov. 21–23
Style RW, Jagota A, Hui CY, Dufresne ER. 2017. Elastocapillarity: surface tension and the mechanics of soft solids. *Annu. Rev. Condens. Matter Phys.* 8:99–118
Sun M, Kumar N, Dhinojwala A, King H. 2021. Attractive forces slow contact formation between deformable bodies underwater. *PNAS* 118:e2104975118
Takagi D, Balmforth NJ. 2011. Peristaltic pumping of rigid objects in an elastic tube. *J. Fluid Mech.* 672:219–44
Tan MR, Wang Y, Frechette J. 2019. Criterion for particle rebound during wet collisions on elastic coatings. *Phys. Rev. Fluids* 4:084305
Tani M, Cambau T, Bico J, Reyssat E. 2017. *Motion of a rigid sphere through an elastic tube with a lubrication film*. Abstract for the March Meeting of the American Physical Society, New Orleans, LA, Mar. 13–17
Tözeren H, Skalak R. 1978. The steady flow of closely fitting incompressible elastic spheres in a tube. *J. Fluid Mech.* 87:1–16
Trouilloud R, Yu TS, Hosoi AE, Lauga E. 2008. Soft swimming: exploiting deformable interfaces for low Reynolds number locomotion. *Phys. Rev. Lett.* 101:048102
Urzay J. 2010. Asymptotic theory of the elastohydrodynamic adhesion and gliding motion of a solid particle over soft and sticky substrates at low Reynolds numbers. *J. Fluid Mech.* 653:391–429
Urzay J, Llewellyn Smith SG, Glover BJ. 2007. The elastohydrodynamic force on a sphere near a soft wall. *Phys. Fluids* 19:103106
Vialar P, Merzeau P, Giasson S, Drummond C. 2019. Compliant surfaces under shear: elastohydrodynamic lift force. *Langmuir* 35:15605–13
Vurgaft A, Elbaz SB, Gat AD. 2019. Forced motion of a cylinder within a liquid-filled elastic tube—a model of minimally invasive medical procedures. *J. Fluid Mech.* 881:1048–72
Wang J, Zhu D. 2019. *Interfacial Mechanics: Theories and Methods for Contact and Lubrication*. Boca Raton, FL: CRC
Wang Y, Dhong C, Frechette J. 2015. Out-of-contact elastohydrodynamic deformation due to lubrication forces. *Phys. Rev. Lett.* 115:248302
Wang Y, Tan MR, Frechette J. 2017. Elastic deformation of soft coatings due to lubrication forces. *Soft Matter* 13:6718–29
Weekley SJ, Waters SL, Jensen OE. 2006. Transient elastohydrodynamic drag on a particle moving near a deformable wall. *Q. J. Mech. Appl. Math.* 59:277–300
Wexler JS, Trinh PH, Berthet H, Quennouz N, du Roure O, et al. 2013. Bending of elastic fibres in viscous flows: the influence of confinement. *J. Fluid Mech.* 720:517–44
Wiertlewski M, Fenton Friesen R, Colgate JE. 2016. Partial squeeze film levitation modulates fingertip friction. *PNAS* 113:9210–15
Wu H, Hui CY, Jagota A. 2023. Solving transient problems in soft elasto-hydrodynamic lubrication. *J. Mech. Phys. Solids* 170:105104
Wu H, Moyle N, Jagota A, Hui CY. 2020. Lubricated steady sliding of a rigid sphere on a soft elastic substrate: hydrodynamic friction in the Hertz limit. *Soft Matter* 16:2760–73
Yang SM, Leal L. 1990. Motions of a fluid drop near a deformable interface. *Int. J. Multiphase Flow* 16:597–616
Yin X, Kumar S. 2005. Lubrication flow between a cavity and a flexible wall. *Phys. Fluids* 17:063101
Zakhari MEA, Bonnecaze RT. 2021. Slip of soft permeable particles near a wall. *Soft Matter* 17:4538–49
Zhang Z, Arshad M, Bertin V, Almohamad S, Raphael E, et al. 2022. Contactless rheology of soft gels over a broad frequency range. *Phys. Rev. Appl.* 17:064045
Zhang Z, Bertin V, Arshad M, Raphael E, Salez T, Maali A. 2020. Direct measurement of the elastohydrodynamic lift force at the nanoscale. *Phys. Rev. Lett.* 124:054502

Zhao H, Spann AP, Shaqfeh ESG. 2011. The dynamics of a vesicle in a wall-bound shear flow. *Phys. Fluids* 23:121901

Zhu D, Wang QJ. 2011. Elastohydrodynamic lubrication: a gateway to interfacial mechanicsreview and prospect. *J. Tribol.* 133:041001

Zilman AG, Granek R. 1996. Undulations and dynamic structure factor of membranes. *Phys. Rev. Lett.* 77:4788–91

Annual Review of Fluid Mechanics

Volume 56, 2024

Contents

Indexes

Errata

An online log of corrections to *Annual Review of Fluid Mechanics* articles may be found at http://www.annualreviews.org/errata/fluid